Draft version December 26, 2016
Preprint typeset using LaTeX style emulateapj v. 01/23/15

arXiv:1612.07885v1 [astro-ph.GA] 23 Dec 2016

TRIGGERING THE FORMATION OF DIRECT COLLAPSE BLACK HOLES BY THEIR CONGENERS

Bin Yue[1,2], Andrea Ferrara[2,3], Fabio Pacucci[2,4], Kazuyuki Omukai[5]
[1]National Astronomical Observatories, Chinese Academy of Sciences, Beijing, 100012, China
[2]Scuola Normale Superiore, Piazza dei Cavalieri 7, I-56126 Pisa, Italy
[3]Kavli IPMU (WPI), Todai Institutes for Advanced Study, the University of Tokyo, Japan
[4]Department of Physics, Yale University, P.O. Box 208101, New Haven, CT 06520, USA and
[5]Astronomical Institute, Tohoku University, Sendai, Miyagi 980-8578, Japan
Draft version December 26, 2016

ABSTRACT

Direct collapse black holes (DCBHs) are excellent candidates as seeds of supermassive black holes (SMBHs) observed at $z \gtrsim 6$. The formation of a DCBH requires a strong external radiation field to suppress H_2 formation and cooling in a collapsing gas cloud. Such strong field is not easily achieved by first stars or normal star-forming galaxies. Here we investigate a scenario in which the previously-formed DCBH can provide the necessary radiation field for the formation of additional ones. Using one-zone model and the simulated DCBH Spectral Energy Distributions (SEDs) filtered through absorbing gas initially having column density $N_{\rm H}$, we derive the critical field intensity, $J_{\rm LW}^{\rm crit}$, to suppress H_2 formation and cooling. For the SED model with $N_{\rm H} = 1.3 \times 10^{25}$ cm^{-2}, 8.0×10^{24} cm^{-2} and 5.0×10^{24} cm^{-2}, we obtain $J_{\rm LW}^{\rm crit} \approx 22$, 35 and 54, all much smaller than for normal star-forming galaxies ($\gtrsim 1000$). X-ray photons from previously-formed DCBHs build up a high-z X-ray background (XRB) that may boost the $J_{\rm LW}^{\rm crit}$. However, we find that in the three SED models $J_{\rm LW}^{\rm crit}$ only increases to ≈ 80, 170 and 390 respectively even when $\dot{\rho}_\bullet$ reaches the maximum value allowed by the present-day XRB level ($0.22, 0.034, 0.006$ $M_\odot {\rm yr}^{-1}{\rm Mpc}^{-3}$), still much smaller than the galactic value. Although considering the XRB from first galaxies may further increase $J_{\rm LW}^{\rm crit}$, we conclude that our investigation supports a scenario in which DCBH may be more abundant than predicted by models only including galaxies as external radiation sources.

Subject headings: dark ages, reionization, first stars – quasars: supermassive black holes – X-rays: diffuse background

1. INTRODUCTION

The quest for supermassive black holes (SMBHs) at $z \gtrsim 6$ has been a remarkable success (Fan et al. 2003; Jiang et al. 2007; Kurk et al. 2007; Mortlock et al. 2011; Morganson et al. 2012; Venemans et al. 2013; Wu et al. 2015). However, the detection of such SMBHs as massive as $\sim 10^9 - 10^{10}$ $M_\odot$ at such early epochs with cosmic age $\lesssim 1$ Gyr has opened a number of questions that remain essentially unanswered.

Black holes (BHs) grow from an initial seed by accreting the surrounding gas. Naive SMBH seed candidates are stellar-mass BHs formed after the death of massive (possibly Pop III) stars, with a typical mass ~ 100 $M_\odot$ or even smaller (Heger et al. 2003; Hosokawa et al. 2011). However, even assuming a continuous accretion at the Eddington limit, the time required to grow a $\sim 10^9$ $M_\odot$ SMBH by $z \sim 6$ is comparable or even longer than the Hubble time at that redshift. Even worse, in the early evolutionary stages, radiative feedback reduces the accretion rate significantly. As a result, for most of the time the BH grows slowly (Alvarez et al. 2009; Jeon et al. 2012; Valiante et al. 2016). Furthermore, reionization of the intergalactic medium (IGM) may also significantly hamper the growth process (Tanaka et al. 2012).

To overcome these problems, an alternative scenario in which a SMBH grows from a seed more massive than 10^4 $M_\odot$ has become popular (see e.g. review Volonteri 2010). Such massive seeds are nicely produced by the so-called "direct collapse" process occurring in metal-free atomic-cooling halos with virial temperature $T_{\rm vir} \gtrsim 10^4$ K (Bromm & Loeb 2003; Koushiappas et al. 2004; Lodato & Natarajan 2006; Begelman et al. 2006, 2008; Begelman 2010; Regan & Haehnelt 2009; Johnson et al. 2013; Latif et al. 2013a,b, 2016; Latif & Ferrara 2016; Latif et al. 2015, 2014; Habouzit et al. 2016; Agarwal et al. 2016b, 2012, 2013, 2014; Choi et al. 2015; Regan et al. 2014; Pacucci et al. 2015a,b; Pacucci & Ferrara 2015). If in these halos H_2 formation and cooling is suppressed, metal-free gas can only cool via Lyα radiation that becomes inefficient when the gas cools below $\sim$ 8000 K. Then, the gas contracts almost isothermally with $T \sim 8000$ K and avoids fragmentation during the cloud collapse (Inayoshi et al. 2014). Eventually at the center a BH with mass $\sim 10^4 - 10^6$ $M_\odot$ forms (Ferrara et al. 2014). Thereafter such a direct collapse black hole (DCBH) continues to accrete the gas and may merge with other BHs. A fully-fledged SMBH is then produced in time scale much shorter than the Hubble time.

The suppression of H_2 formation requires either a strong Lyman-Werner (LW, $11.2 < h\nu < 13.6$ eV) UV radiation field that directly dissociates H_2, or a strong continuum radiation field from near-infrared (NIR) to UV band ($0.755 < h\nu < 13.6$ eV) that detaches the most important H_2 formation catalyst, H^-. The required critical field intensity and the clustering of the dark matter halos

yuebin@bao.ac.cn

determine the actual abundance of DCBHs in high-z Universe (Dijkstra et al. 2008; Yue et al. 2014). The DCBH abundance has been studied by many authors and the predicted number density at $z \sim 10$ ranges from $\sim 10^{-10}$ Mpc^{-3} to $\sim 10^{-3}$ Mpc^{-3} (e.g. Agarwal et al. 2012, 2013; Dijkstra et al. 2014; Pacucci et al. 2015a; Habouzit et al. 2016). Nevertheless such number density is much smaller than that of galaxies in the high-z Universe.

Generally, in this scenario the required critical field intensity is very high. For an ideal blackbody spectrum with effective temperature 10^4 K, $J^{\rm crit}_{\nu_{13.6}} \sim 30-300$ (Omukai 2001; Shang et al. 2010); for a realistic galaxy spectrum $J^{\rm crit}_{\nu_{13.6}} \gtrsim 1000-10000$ (Sugimura et al. 2014; Latif et al. 2015), where $J_{\nu_{13.6}}$ is the specific intensity of the radiation field at 13.6 eV and in units 10^{-21} erg $\mathrm{s}^{-1}\mathrm{cm}^{-2}\mathrm{Hz}^{-1}\mathrm{sr}^{-1}$. Such a strong radiation field can be attained only when the radiation source is very close to the DCBH-forming gas cloud. In spite of this stringent requirement, the discovery of two high-z DCBH candidates in the CANDELS/GOODS-S survey has been recently reported (Pacucci et al. 2016). Moreover, the Lyman alpha emitter (LAE) "CR7" has been observed and reported as a DCBH candidate by some authors, because its strong Lyα and HeII 1640 Å line luminosities are hard to be provided by Pop III stars; and the two nearby Pop II galaxies are ideal sources for providing strong external radiation, although this detection is still a matter of debate (Sobral et al. 2015; Pallottini et al. 2015; Smith et al. 2016; Agarwal et al. 2016a; Smidt et al. 2016; Bowler et al. 2016; Pacucci et al. 2016, in prep).

In Yue et al. (2014) we proposed that an accreting and Compton-thick DCBH can provide a radiation field that suppresses H_2 formation in a more efficient way compared with a galaxy. The advantages here are: the ratio of the H^- photo-detachment rate to the H_2 photo-dissociation rate is a most straightforward indicator of the H_2 suppression efficiency (Sugimura et al. 2014; Wolcott-Green et al. 2016), for the Spectral Energy Distribution (SED) of a Compton-thick DCBH this ratio is higher than for normal star-forming galaxies; and a BH is usually brighter than a galaxy. Moreover, there is an additional advantage: if the source also produces X-ray and ionizing photons, in general it may hamper DCBH formation (Glover 2016; Regan et al. 2016; Aykutalp et al. 2014; Inayoshi & Tanaka 2015; Johnson et al. 2014; Inayoshi & Omukai 2011); however if the source is a Compton-thick DCBH, except a few very hard X-ray photons (i.e. $\gtrsim$ 10 keV) during most of the accretion stage it does not emit X-rays and ionizing photons. In this case, the abundance of high-z DCBHs can be higher than currently expected.

In this work, we derive the critical field intensity for the formation of a new DCBH inside a collapsing gas cloud irradiated by a nearby previously-formed DCBH by means of the one-zone model in which the whole cloud is assumed to have uniform properties. The SEDs of the DCBH are taken from numerical simulations (Pacucci et al. 2015a). We consider three SED models with *initial* column number densities $N_{\rm H} = 1.3 \times 10^{25}$ cm^{-2}, $N_{\rm H} = 8.0 \times 10^{24}$ cm^{-2} and $N_{\rm H} = 5.0 \times 10^{24}$ cm^{-2} respectively. Throughout this paper $N_{\rm H}$ refers to the column number density of the gas envelope that encloses the accretion disc, at the time when accretion just starts. The real column density filtering the BH radiation is time-dependent and decreases as accretion processes.

Regarding the X-ray radiation, although during most of its accretion process the nearby DCBH only emits hard X-ray photons that negligibly influence the H_2 formation, the collective X-ray emission[1] from distant DCBHs and galaxies builds up a high-z X-ray background (XRB) that ionizes the gas and may promote the H_2 formation. We also investigate the impact of such high-z XRB on the DCBH formation.

The layout of this paper is as follows. In Section 2 we introduce the one-zone model and the DCBH SEDs. In Section 3 we present the results, including tests of our code for a pure blackbody spectrum and for a normal star-forming galaxy spectrum; the critical field intensities for DCBH SEDs and their variance when the XRB is considered. We give the conclusions and discussions in Section 4. In Appendix A we compare the optical depth of the DCBH-forming gas cloud to the LW radiation, to the H^- detachment radiation and to the H_2^+ dissociation radiation. In Appendix B we present discussions on enhanced DCBH formation probability. In Appendix C we list the chemical reactions and heating/cooling functions included in our chemistry network. Throughout the paper, we use the `Planck` cosmology parameters (Planck Collaboration et al. 2015): Ω_m=0.308, Ω_Λ=0.692, h=0.6781, Ω_b=0.0484, n = 0.9677 and σ_8=0.8149. The transfer function is from Eisenstein & Hu (1998).

2. METHODS

2.1. *The one-zone model*

The one-zone model developed here describes the evolution of a gas cloud that eventually collapses to form a Pop III star, a galaxy or a BH. Similar approaches have been successfully applied to a variety of problems (see e.g. Omukai 2000, 2001; Omukai et al. 2005; Sugimura et al. 2014; Visbal et al. 2014; Inayoshi & Tanaka 2015; Stacy & Bromm 2007).

2.1.1. *Halo build up*

The formation of a dark matter halo is described by the "top-hat" spherical collapse scenario, in which the dark matter density $\rho_{\rm d}$ evolves as

$$\rho_{\rm d} = \begin{cases} \dfrac{9\pi^2}{2}\left(\dfrac{1+z_{\rm ta}}{1-\cos\theta}\right)^3 \rho_c(\Omega_m-\Omega_b) & z > z_{\rm halt} \\ \dfrac{9\pi^2}{2}(1+z_{\rm ta})^3\rho_c(\Omega_m-\Omega_b) & z \le z_{\rm halt}, \end{cases} \quad (1)$$

where ρ_c is the Universe critical density and $z_{\rm ta}$ is the turn-around redshift; θ is linked to redshift via

$$\theta - \sin\theta = \pi\left(\frac{1+z_{\rm ta}}{1+z}\right)^{3/2}, \quad (2)$$

[1] Generally soft X-ray photons are trapped in the high column density matter and only hard X-ray photons contribute to the XRB. However, as the matter is swallowed by the DCBH the column density decreases, eventually soft X-ray photons can also escape from the BH (Pacucci et al. 2015a) and contribute to the XRB as well.

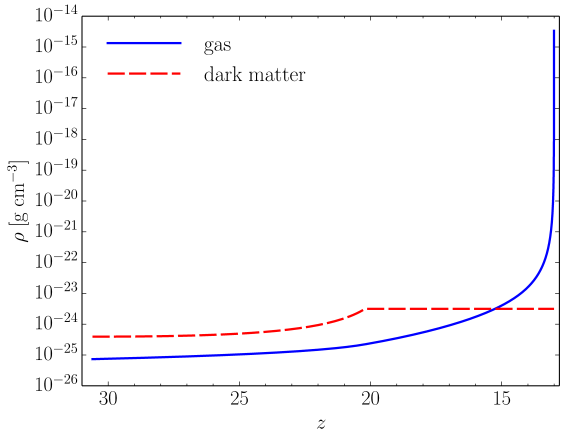

FIG. 1.— The density evolution of dark matter and collapsing gas cloud in a dark matter halo with turn-around redshift 30.6.

and by halting the density evolution at the redshift corresponding to $\theta_{\rm halt} = 3\pi/2$, we force the dark matter density not to exceed the final virialization density[2]

The dark matter halo provides the gravity that promotes its gas content to collapse. Ignoring the pressure, the gas density $\rho_{\rm g}$ evolves as

$$\frac{d\rho_{\rm g}}{dt} = \frac{\rho_{\rm g}}{t_{\rm ff}}, \tag{3}$$

where the free-fall time scale

$$t_{\rm ff} = \sqrt{\frac{3\pi}{32G(\rho_{\rm d}+\rho_{\rm g})}}. \tag{4}$$

Throughout this paper we investigate a halo with $z_{\rm ta} = 30.6$; its gas eventually collapses to form a galaxy or DCBH at $z \sim 13$. In Fig. 1 we plot the evolution of the dark matter and gas density, where the initial gas density is set to be $\Omega_b/(\Omega_m - \Omega_b)\rho_{\rm d}(z_{\rm ta})$. This dark matter collapse gets halted at $z \sim 20.5$ and the gas density exceeds the dark matter density at $z \sim 15$.

2.1.2. *Temperature evolution*

The temperature of the cloud is followed by solving the energy equation

$$\frac{1}{T}\frac{dT}{dt} = (\gamma-1)\frac{1}{\rho_{\rm g}}\frac{d\rho_{\rm g}}{dt} + \frac{1}{\mu}\frac{d\mu}{dt} + (\gamma-1)\frac{\mathcal{H}-\Lambda}{nk_{\rm B}T}, \tag{5}$$

where $\gamma = 5/3$ is the adiabatic index for the monatomic gas, $k_{\rm B}$ is the Boltzmann constant, μ is the molecular weight and $n = \rho_{\rm g}/\mu$ is the sum of the number density of all the eight species; $\mathcal{H}$ and Λ are the heating and cooling rates per unit volume, respectively.

Even in the pre-reionization epoch, X-ray photons can propagate over long distances and heat the gas with a rate

$$\mathcal{H}_{\rm X} = f_{\mathcal{H}}\mathcal{E}, \tag{6}$$

[2] In the literature, in the top-hat spherical collapse scenario, usually the "virialization redshift" refers to the "collapse redshift", i.e. the redshift corresponding to $\theta_{\rm vir} = 2\pi$ when the density approaches infinity. However this singularity does not happen in practice, since the gas collapse gets halted well before it.

where $\mathcal{E}$ is the energy (per unit time and volume) of primary electrons due to X-ray ionization, while $f_{\mathcal{H}}$ is the fraction of the primary energy deposited as thermal energy and we use the value by Valdés & Ferrara (2008) (see Shull & van Steenberg 1985 as well). The primary electron energy (here we ignore the photoionization of He^+)

$$\mathcal{E} = \int_{0.1\ {\rm keV}} dE \frac{4\pi J_X(E) e^{-\tau_{\rm cl}(E)}}{E} \sum_{i={\rm H,He}} (E-E_i)\sigma_i(E) n_i \tag{7}$$

where J_X is the specific intensity of the X-ray background (see Sec. 3.3), $E_{\rm H} = 13.6$ eV and $E_{\rm He} = 24.6$ eV are the ionization potentials for H and He, respectively. The photo-electric cross-section, $\sigma_{\rm H}(E)$ and $\sigma_{\rm He}(E)$, are from Balucinska-Church & McCammon (1992). The optical depth of the gas cloud is given as

$$\tau_{\rm cl}(E) = \sum_{i={\rm H,He}} \sigma_i(E) n_i \lambda_J/2, \tag{8}$$

by using the cloud Jeans length λ_J.

In addition to the X-ray heating, we also take into account the heating associated with chemical reactions listed in Table 4 in Appendix C. However, throughout this paper we are concerned with DCBH formation in the pre-reionization epoch, when the neutral IGM is opaque to UV photons, we hence ignore the ionization and heating by them.

For the cooling rate Λ, we include the radiative cooling by H_2, H, He, and He^+, and cooling associated with chemical reactions. The cooling functions for individual processes are also listed in Table 5 in Appendix C.

We stop our calculations at $n \sim 10^9$ cm^{-3}, because our treatment of H_2 cooling is only valid for number densities $\lesssim 10^9$ cm^{-3} when the gas is optically thin to H_2 lines (e.g. Yoshida et al. 2006). However, according to some previous works (e.g. Omukai 2001), which investigated the subsequent evolution up to density $\gg 10^9$ cm^{-3}, we can conclude that, as long as the H_2 formation have been suppressed in a cloud before density reaches $\sim 10^4$ cm^{-3}, H_2 is collisionlly dissociated in higher density and the cloud continues to collapse only via the atomic cooling. This will result in the formation of a supermassive star at the center, which will then collapses to a BH (Umeda et al. 2016).

2.2. *Chemical Reactions*

We consider the evolution of eight chemical species H^-, H, H^+, H_2, H_2^+, He, He^+ and e^- (we ignore the He^{++} since it plays a negligible role) by using the reaction rates listed in Table 3 in Appendix C. The reaction rates are collected from Palla et al. (1983); Omukai (2000); Glover & Abel (2008); Shang et al. (2010) and the original references are found in them. In a cloud irradiated by an external radiation field, H_2 formation is suppressed via the following three reactions: H_2 photodissociation

$$H_2 + \gamma \xrightarrow{k_{\rm H_2,dis}} 2H, \tag{9}$$

H^- photo-detachment

$$H^- + \gamma \xrightarrow{k_{\rm H^-,det}} H + e^- \tag{10}$$

and H_2^+ photo-dissociation

$$H_2{}^+ + \gamma \xrightarrow{k_{H_2^+,\rm dis}} H + H^+ \quad (11)$$

respectively, where $k_{\rm H_2,dis}, k_{\rm H^-,det}$ and $k_{\rm H_2^+,dis}$ are the corresponding reaction rates (i.e., k_{22}, k_{23}, and k_{24} in Table 3). The photo-dissociation and photo-detachement rates of H_2, H^- and H_2^+ are described below in Sec. 2.2.1, 2.2.2 and 2.2.3 respectively. We consider the photo-ionization only by the X-ray background (Sec. 2.2.4), and ignore all reactions that need ionizing photons other than X-rays.

2.2.1. *Photo-dissociation of* H_2

Photons in the narrow LW band can dissociate the H_2 through the two-step Solomon process (e.g., Stecher & Williams 1967). The ground electronic state H_2 $X(v''=0, J'')$ are excited to the state $B(v', J')$ by absorbing the photons in the Lyman band, or to the state $C(v', J')$ by absorbing the photons in the Werner band. A fraction of these excited molecules decays to high ($v'' \geq 14$) vibrational levels and then dissociates to separate atoms. The photo-dissociation rate is then (Abel et al. 1997)

$$k_{\rm H_2,dis} = \sum \frac{\pi e^2}{m_e c} p_{i'} f_{i'} \int \frac{4\pi J(\nu)}{h\nu} \phi_{i'}(\nu - \nu_{i'}) d\nu, \quad (12)$$

where $J(\nu)$ is the specific intensity of the external radiation field at frequency ν, $p_{i'}$ the probability of the transition from the ground state to $B(\nu', J')$ or $C(\nu', J')$ (Abgrall & Roueff 1989), $f_{i'}$ the dissociation fraction (Abgrall et al. 1992), $\nu_{i'}$ the frequency of the transition emission line, which has normalized profile $\phi_{i'}(\nu - \nu_{i'})$, and $\pi e^2/(m_e c) = 2.65 \times 10^{-2}$ cm^2. We assume that the ground-state hydrogen molecules are para-H_2 with $J''=0$ (Abel et al. 1997). In case the line profile is a Dirac δ function, the above equation reduces to

$$k_{\rm H_2,dis} \approx \sum \frac{\pi e^2}{m_e c} p_{i'} f_{i'} \frac{4\pi J(\nu_{i'})}{h\nu_{i'}}. \quad (13)$$

The sum is performed for all possible transitions with transition energy smaller than 13.6 eV.

For a blackbody radiation field with effective temperature 10^4 K ("BB") and with mean specific intensity $J_{\rm LW} \times 10^{-21}$ erg s^{-1}cm^{-2}Hz^{-1} sr^{-1} in the LW band[3], we have

$$k^{\rm BB}_{\rm H_2,dis} = 7.74 \times 10^{-13} J_{\rm LW} f_{\rm sh}\ [{\rm s}^{-1}], \quad (14)$$

where the self-shielding effect is included by the self-shielding parameter (Wolcott-Green et al. 2011)

$$f_{\rm sh} = \frac{0.965}{(1+x/b_5)^{1.1}} + \frac{0.035}{(1+x)^{0.5}} \exp\left[-8.5\times10^{-4}(1+x)^{0.5}\right], \quad (15)$$

in which $x = N_{\rm H_2}/5\times10^{14}$ cm^{-2} is the H_2 column number density $N_{\rm H_2}$ in units 5×10^{14} cm^{-2}; and b_5 is the Doppler broadening parameter in units 10^5 cm s^{-1}

$$b_5 = \frac{\sqrt{2k_{\rm B}T/m_{\rm H_2}}}{10^5 \text{ cm s}^{-1}}; \quad (16)$$

and $m_{\rm H_2}$ is the hydrogen molecule mass. We ignore the micro-turbulent velocity, therefore the self-shielding effect is possibly overestimated here (Glover & Brand 2001). The H_2 column density is given by $N_{\rm H_2} = n_{\rm H_2}\lambda_J/2$, where λ_J is the Jeans length of the gas cloud.

For a star-forming galaxy spectrum ("GAL") with mean LW specific intensity $J_{\rm LW}$,

$$k^{\rm GAL}_{\rm H_2,dis} = 1.23\times10^{-12} J_{\rm LW} f_{\rm sh}\ [{\rm s}^{-1}]. \quad (17)$$

Here, we take the star-forming galaxy spectrum from `STARBURST99`[4] (Leitherer et al. 1999; Vázquez & Leitherer 2005; Leitherer et al. 2010) and adopt the continuous star formation mode, Salpeter initial mass function (IMF) with mass range of 0.1 - 100 $M_\odot$, metallicity of 0.02 $Z_\odot$ and the age of 100 Myr.

For a Compton-thick DCBH, most photons in the UV to soft X-ray bands are absorbed by the thick envelope enclosing the accretion disc, then re-emitted at the energies below 13.6 eV in the form of Lyα emission, two-photon emission, free-free and free-bound emission, respectively. Therefore its SED has two main components: the remaining unabsorbed photons (hard X-rays and the <13.6 eV part of the multi-color blackbody radiation) and the re-processed photons. The relative weight of these two components depends on the column number density of the Compton-thick matter.

Using numerical simulations Pacucci et al. (2015a) have carefully investigated the radiation from DCBHs. They obtained the SEDs for different $N_{\rm H}$ values. In Fig. 2 we show the SEDs of Compton-thick DCBH with $N_{\rm H} = 1.3\times10^{25}$ cm^{-2} ("BH1"), 8.0×10^{24} cm^{-2} ("BH2") and 5.0×10^{24} cm^{-2} ("BH3") respectively, at the time 10 Myr after the accretion starts. They are for the standard disk, LDP density profile, see Pacucci et al. (2015a) for details. We only plot the energy range relevant to the H_2 chemistry, ignoring the >13.6 eV part. For all the three SEDs the two-photon emission is the dominant radiation from $\sim$ 3 eV to $\sim$11.2 eV, below the $\sim$ 3 eV the free-bound emission dominates over others. The higher the $N_{\rm H}$, the more energy is re-processed to the <13.6 eV part, and such SED is expected to suppress the H_2 formation more efficiently. In case the envelope is rather thick, i.e. $N_{\rm H} \gtrsim 10^{25}$ cm^{-2}, Lyα emission is barely seen as the corresponding photons are well-trapped in the thick envelope and, finally most of them escape from the envelope as two-photon emission.

The SED obtained in Pacucci et al. (2015a) evolves as the accretion progresses. However, for the BH mass investigated in this paper the SED is always stationary when the accretion time is smaller than $\sim$ 100 Myr, only the normalization changes with the increasing BH mass. In our work we always use the SEDs plotted in Fig. 2 as the spectrum of the external radiation field, leaving the normalization as a free parameter representing the

[3] Note that in the literature sometimes the radiation field strength is represented by different quantities. For example, in Abel et al. (1997) the specific intensity at 12.87 eV is used, while Shang et al. (2010) uses the specific intensity at 13.6 eV. We use the *mean* LW specific intensity instead of the specific intensity at a given energy because our DCBH SEDs are not flat in the LW band and because of the presence of several emission lines in this band.

[4] http://www.stsci.edu/science/starburst99/docs/default.htm

different distances from the collapsing gas cloud to the nearby emitting DCBH.

For comparison the BB and GAL spectra are also shown in Fig. 2. All SEDs there have $J_{\rm LW} = 1.0$. Substituting the DCBH SEDs into Eq. (13), we find all the three DCBH models have almost the same H_2 photo-dissociation rate

$$k^{\rm BH}_{\rm H_2,dis} = 1.30 \times 10^{-12} J_{\rm LW} f_{\rm sh}\ [{\rm s}^{-1}]. \quad (18)$$

2.2.2. *Photo-detachment of* H^-

The H^- could be detached by photons in the wide energy range of 0.755 - 13.6 eV. The reaction rate is obtained through integration,

$$k_{\rm H^-,det} = \int_{\nu_{0.755}}^{\nu_{13.6}} \frac{4\pi J(\nu)}{h\nu} \sigma_{\rm H^-,det}(\nu) d\nu, \quad (19)$$

where the cross-section is (Abel et al. 1997)

$$\sigma_{\rm H^-,det}(\nu) = 7.928 \times 10^5 (\nu - \nu_{0.755})^{1.5}/\nu^3\ [{\rm cm}^2]; \quad (20)$$

$\nu_{0.755}$ is the frequency (in Hz) of a photon with energy 0.755 eV and $\nu_{13.6}$ with 13.6 eV. For the BB and GAL radiation fields with mean LW specific intensity $J_{\rm LW}$, we obtain[5]

$$k^{\rm BB}_{\rm H^-,det} = 5.60 \times 10^{-8} J_{\rm LW}\ [{\rm s}^{-1}], \quad (21)$$

and

$$k^{\rm GAL}_{\rm H^-,det} = 5.43 \times 10^{-11} J_{\rm LW}\ [{\rm s}^{-1}]. \quad (22)$$

For DCBH SEDs,

$$\begin{aligned} k^{\rm BH1}_{\rm H^-,det} &= 5.27 \times 10^{-8} J_{\rm LW}\ [{\rm s}^{-1}] \\ k^{\rm BH2}_{\rm H^-,det} &= 1.87 \times 10^{-8} J_{\rm LW}\ [{\rm s}^{-1}] \\ k^{\rm BH3}_{\rm H^-,det} &= 6.29 \times 10^{-9} J_{\rm LW}\ [{\rm s}^{-1}]. \end{aligned} \quad (23)$$

Apparently, $k^{\rm BH1}_{\rm H^-,det} \approx k^{\rm BB}_{\rm H^-,det} \gg k^{\rm GAL}_{\rm H^-,det}$, and since this is the most relevant reaction suppressing the H_2 formation, we therefore expect the critical specific intensity, $J^{\rm crit}_{\rm LW}$, for a BH1 radiation field, to be comparable with a BB radiation field while much smaller than a GAL radiation field.

2.2.3. *Photo-dissociation of* H_2^+

H_2^+ is dissociated by photons above 2.65 eV. The reaction has a cross-section (Shapiro & Kang 1987) given by

$$\log(\sigma_{\rm H_2^+}) = \begin{cases} -40.97 + 6.03E_\gamma - 0.504E_\gamma^2 + 1.387 \times 10^{-2} E_\gamma^3 \\ \qquad\qquad (2.65 < E_\gamma < 11.27) \\ -30.26 + 2.79E_\gamma - 0.184E_\gamma^2 + 3.535 \times 10^{-3} E_\gamma^3 \\ \qquad\qquad (11.27 < E_\gamma < 21) \end{cases}$$

where E_γ and the cross-section are in units eV and $\rm cm^2$ respectively. Similar to Eq. (19), we get the reaction rate for the BB and GAL radiation fields

$$k^{\rm BB}_{\rm H_2^+,dis} = 4.30 \times 10^{-11} J_{\rm LW}\ [{\rm s}^{-1}], \quad (24)$$

[5] Here the mean LW specific intensity, $J_{\rm LW}$, is only used to denote the normalization of the SED, actually all photons with energy $\gtrsim 0.755$ eV detach the H^-.

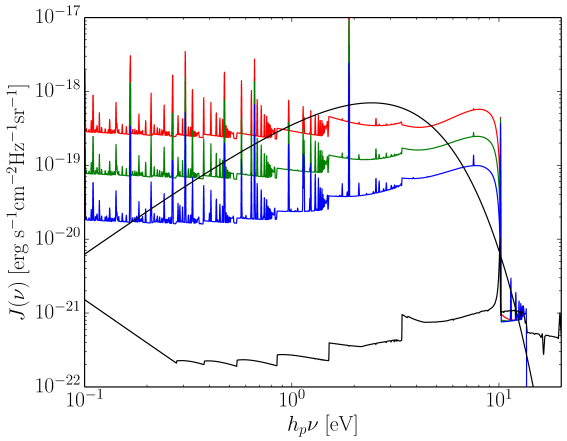

FIG. 2.— The DCBH SEDs (from top to bottom, the three curves with emission lines correspond to BH1, BH2 and BH3 respectively), compared with a blackbody spectrum with effective temperature 10^4 K (smooth curves) and a star-forming galaxy spectrum (bottom curve with sawteeth).

and

$$k^{\rm GAL}_{\rm H_2^+,dis} = 6.25 \times 10^{-12} J_{\rm LW}\ [{\rm s}^{-1}]. \quad (25)$$

For DCBH SEDs

$$\begin{aligned} k^{\rm BH1}_{\rm H_2^+,dis} &= 8.61 \times 10^{-10} J_{\rm LW}\ [{\rm s}^{-1}] \\ k^{\rm BH2}_{\rm H_2^+,dis} &= 3.63 \times 10^{-10} J_{\rm LW}\ [{\rm s}^{-1}] \\ k^{\rm BH3}_{\rm H_2^+,dis} &= 1.46 \times 10^{-10} J_{\rm LW}\ [{\rm s}^{-1}]. \end{aligned} \quad (26)$$

We have confirmed that the gas cloud is always transparent to both H^- detachment radiation and H_2^+ dissociation radiation and neglect their shielding effect, see a check in Appendix A.

2.2.4. *Photo-ionization of* H *and* He *by X-rays*

The total ionization rate of hydrogen atoms, including photoionization and secondary ionizations, is

$$\mathcal{I}_{\rm H} = \int dE \frac{4\pi J(E) e^{-\tau_{\rm cl}(E)}}{E} \sigma_{\rm H}(E) n_{\rm H} + \frac{f_{\mathcal{I},{\rm H}} \mathcal{E}}{E_{\rm H}}, \quad (27)$$

and of the helium atoms is

$$\mathcal{I}_{\rm He} = \int dE \frac{4\pi J(E) e^{-\tau_{\rm cl}(E)}}{E} \sigma_{\rm He}(E) n_{\rm He} + \frac{f_{\mathcal{I},{\rm He}} \mathcal{E}}{E_{\rm He}}, \quad (28)$$

where $f_{\mathcal{I},{\rm H}}$ and $f_{\mathcal{I},{\rm He}}$ are fractions of primary energy deposited into hydrogen secondary ionization and helium secondary ionization respectively and are from Valdés & Ferrara (2008).

2.2.5. *Numerical Approach*

The initial temperature is set to be the adiabatic temperature of the IGM at $z_{\rm ta}$ (Barkana & Loeb 2001). The initial H_2 fraction, i.e. the H_2 number density to H and H^+ number density ratio, is set to be 10^{-6} (Lepp & Shull 1984; Hirata & Padmanabhan 2006); the initial H^+ fraction and He^+ fraction are all set to be 10^{-4}, and the initial electron fraction is their sum; fractions of other species are set to be zero.

We solve the differential equations of the chemistry network together with Eq. (3) and Eq. (5) starting from

$z_{\rm ta}$, to obtain the evolution of gas density, temperature and chemical abundances. To guarantee the precision we force the time-step to be the 0.1% of the minimum of all $y_i/(dy_i/dt)$, where dy_i/dt is the derivative of the ith differential equation excluding $d{\rm H}^-/dt$ and $d{\rm H}_2^+/dt$ (see below). The reaction rates for the intermediary species, H^- and H_2^+, are much larger than for the other species. Hence, to reduce the computational time, we always use equilibrium abundances for H^- and H_2^+ obtained by iteratively solving the following simultaneous equations:

$$
\begin{aligned}
n_{\rm H^-}^{\rm eq} &= (k_7 n_{\rm H} n_e + k_{12} n_{\rm H_2} n_e)/(k_8 n_{\rm H} + k_{10} n_{\rm H_2^+}^{\rm eq} + k_{11} n_{\rm H^+} \\
&\quad + k_{17} n_{\rm e} + k_{18} n_{\rm H} + k_{19} n_{\rm H^+} + k_{\rm H^-,det}), \\
n_{\rm H_2^+}^{\rm eq} &= (k_5 n_{\rm H} n_{\rm H^+} + k_{15} n_{\rm H_2} n_{\rm H^+} + k_{19} n_{\rm H^-}^{\rm eq} n_{\rm H^+})/(k_6 n_{\rm H} \\
&\quad + k_9 n_{\rm e} + k_{10} n_{\rm H^-}^{\rm eq} + k_{\rm H_2^+,dis}).
\end{aligned} \tag{29}
$$

The validity of this treatment has been proven by previous works (e.g. Abel et al. 1997; Omukai & Nishi 1998; Bromm et al. 2002; Omukai et al. 2010).

3. RESULTS

3.1. *The critical intensity for the blackbody and galactic spectra: Tests of the code*

First, we run the code for a collapsing gas cloud irradiated by the BB and the GAL radiation fields as a test. Here we ignore the XRB.

For the BB radiation field with different strengths, the temperature, the H_2 and e^- fractions are plotted in upper and bottom panels of Fig. 3, respectively. In the absence of an external radiation field or when the radiation field is weak (e.g. $J_{\rm LW} = 1$), the gas cloud cools by H_2 and attains a temperature $\sim 250 - 300$ K at $n \sim 10^3$ cm^{-3}, where the H_2 rotational levels reach the local thermodynamic equilibrium. At higher densities, H_2 cooling rate saturates and the temperature increases gradually, reaching ~ 800 K at $n \sim 10^9$ cm^{-3}, consistent with previous studies (Omukai 2001). On the other hand, with a more intense field, i.e., $J_{\rm LW} = 30$, the H_2 formation and cooling are suppressed, and up to $n \sim 10^9$ cm^{-3} the evolution remains quasi-isothermal at $T \gtrsim 6000$ K set by atomic-cooling mechanism.

The blackbody spectrum with effective temperature 10^4 K has $J_{\rm LW}/J_{\nu_{13.6}} = 3.69$. Hence $J_{\rm LW}^{\rm crit} = 30$ is translated into $J_{\nu_{13.6}}^{\rm crit} = 8$. This is smaller than Shang et al. (2010) who found $J_{\nu_{13.6}}^{\rm crit} = 39$. Latif et al. (2014); Glover (2015) pointed out that Shang et al. (2010) ignored the dissociative tunneling effect term in Martin et al. (1996), as a result their H_2 collisional dissociation rate is underestimated. Our critical value is even smaller than Glover (2015) who got $J_{\nu_{13.6}}^{\rm crit} \approx 17$. We have checked that such discrepancy is due to the different initial setups. Using the same initial setups, and using $N_{\rm H_2} = n_{\rm H_2}\lambda_J$ instead of $N_{\rm H_2} = n_{\rm H_2}\lambda_J/2$, we get $J_{\nu_{13.6}}^{\rm crit} = 16$, very close to Glover (2015). We further test the same initial setups as Inayoshi & Omukai (2011), and consistently get $J_{\nu_{13.6}}^{\rm crit} = 16$.

In addition to the BB radiation field, we also check the GAL field, and find that when $J_{\rm LW} \gtrsim 700$, the H_2 formation and cooling is suppressed.

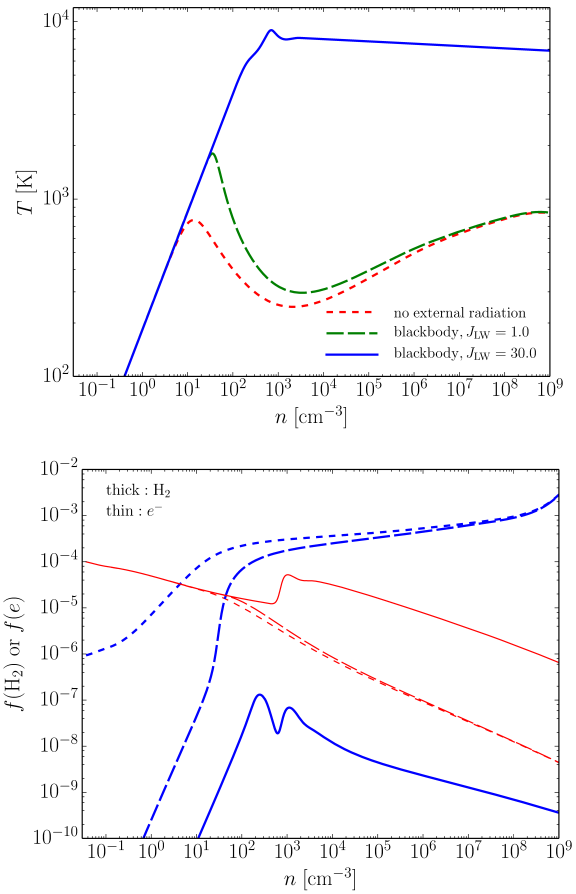

FIG. 3.— *Upper panel:* Temperature evolution as a function of gas density for a gas cloud irradiated by an external BB radiation field with different $J_{\rm LW}$ values. *Bottom:* Evolution of the H_2 (thick lines) and e^- (thin lines) fractions for the BB model.

3.2. *The critical intensity by DCBHs: cases without X-ray background*

In Fig. 4, we show the temperature evolution of a collapsing gas cloud irradiated by the BH1 radiation field, for different field strengths, which corresponds to different distances to the source DCBH. For this model, we find $J_{\rm LW}^{\rm crit} \approx 22$ and, as expected, it is similar to the BB radiation since $k_{\rm H^-,det}^{\rm BB} \approx k_{\rm H^-,det}^{\rm BH1}$. For the BH2 and BH3 spectra, we find $J_{\rm LW}^{\rm crit} \approx 35$ and $J_{\rm LW}^{\rm crit} \approx 54$, respectively.

In the above calculations the external radiation field is turned on from the initial phase, i.e. $z_{\rm ta} = 30.6$, to the final collapse redshift, i.e. $z_{\rm fin} = 13$. The time interval between these two epochs is ≈ 233 Myr. This might raise some concern as such time span is longer than the typical DCBH accretion time, ~ 100 Myr. We note, however, that such a long irradiation time is not really necessary. For most of the time the gas density and temperature remain around the initial values. Later on, the cumulative H_2 formed during this early evolutionary stages will be easily washed out by external radiation field as long as it can penetrate into the gas cloud.

We now examine the minimal requirement for the irradiation time. For this purpose, we initially set the external radiation to be zero, and switch it on at some gas density $n_{\rm on}$. We then repeat the calculations for dif-

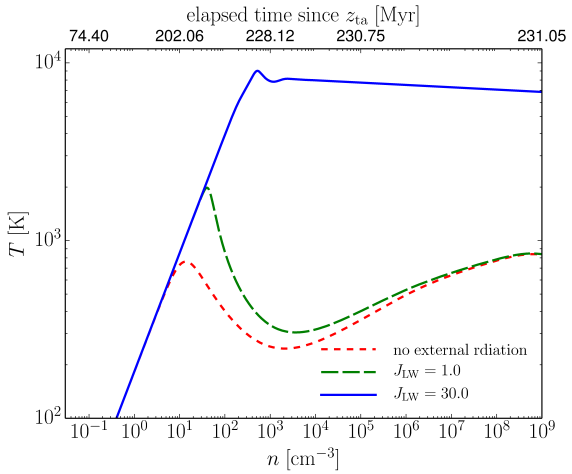

FIG. 4.— Temperature evolution for the gas cloud irradiated by the BH1 radiation field with different strengths. The model without external radiation field is also plotted. We mark the elapsed time since z_{ta} on the upper x-axis.

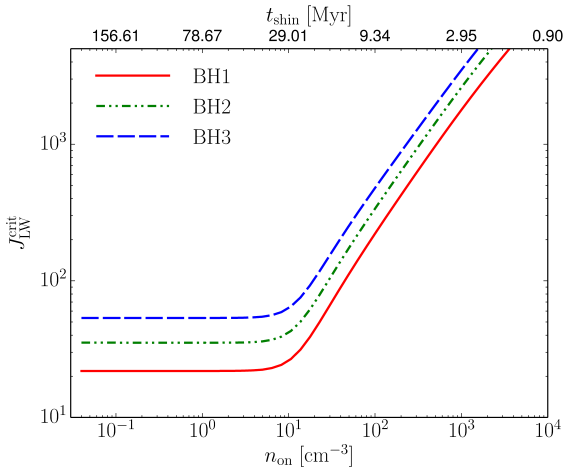

FIG. 5.— The critical intensity J_{LW}^{crit} vs. the density at which the radiation field is switched on, n_{on}, for different DCBH spectra. The shining time is marked on the upper x-axis.

ferent n_{on} values to obtain the dependence of J_{LW}^{crit} on n_{on}. The result is presented in Fig. 5. The shining time t_{shin}, defined as the duration of the irradiation before the final collapse, is also indicated on the upper x-axis. For $n_{on} \lesssim 10$ cm^{-3}, J_{LW}^{crit} remains constant. While for higher n_{on}, the increasingly higher J_{LW}^{crit} is needed for the direct collapse. For example, with the BH1 spectrum, for n_{on} as high as 100 cm^{-3}, J_{LW}^{crit} is raised to ≈ 230. In this case, the cloud can be irradiated only for ~ 9 Myr (from $n = 100$ cm^{-3} to the final collapse). If the external radiation field is switched on at $n_{on} = 1000$ cm^{-3}, the required intensity is even higher, $J_{LW}^{crit} \approx 1800$. In this case external radiation field is only required for ~ 3 Myr.

The J_{LW}^{crit} - n_{on} relation shown in Fig. 5 can be fitted by a formula

$$\log(J_{LW}^{crit}) = c_1 + (1 - e^{-n_{on}/c_2})[c_3 \log(n_{on}) + c_4] \quad (30)$$

for each type of the spectrum and the coefficients $c_1 - c_4$ are presented in Table 1. It may be more convenient

TABLE 1
FITTING COEFFICIENTS FOR J_{LW}^{crit} - n_{on} RELATION

spectrum	c_1	c_2	c_3	c_4
BH1	1.34	23.3	0.83	−0.60
BH2	1.55	22.3	0.82	−0.60
BH3	1.73	21.8	0.80	−0.60

TABLE 2
FITTING COEFFICIENTS FOR J_{LW}^{crit} - t_{shin} RELATION

spectrum	d_1	d_2	d_3	d_4
BH1	1.34	14.6	−1.49	2.65
BH2	1.55	14.5	−1.45	2.59
BH3	1.73	14.5	−1.43	2.53

to know the t_{shin} in some cases, we therefore also fit a formula for the $J_{LW}^{crit} - t_{shin}$ relation,

$$\log(J_{LW}^{crit}) = d_1 + (1 - e^{-d_2/t_{shin}})[d_3 \times \log(t_{shi}) + d_4], \quad (31)$$

parameters are listed in Tab. 2.

3.3. *The impact of an X-ray background*

The XRB ionizes the cloud, producing more free electrons and promoting H_2 formation. As such, it works as a negative feedback on DCBH formation and boost the critical intensity (Inayoshi & Omukai 2011). Here, we study to what extent the critical intensity is modified by the presence of a XRB. We consider two types of the X-ray sources: (i) accreting DCBHs and (ii) first galaxies.

3.3.1. *X-rays from DCBHs*

Since a DCBH is Compton-thick during most of its accretion stage, soft X-rays are absorbed in the envelope. Only hard X-rays come out from the source, which have negligible impacts on a nearby forming DCBH. However, near the end of accretion, with most of the halo gas reservoir having been swallowed by the growing DCBH, some soft X-ray photons can leak out of the system (Pacucci et al. 2015a). Such soft X-rays from DCBHs cumulatively builds up a high-z XRB.

We first derive the XRB spectrum from accreting DCBHs. Assuming that the DCBH formation rate is proportional to the formation rate of atomic-cooling halos with the virial temperature in range 10000 K $< T_{vir} <$ 20000 K, the DCBH X-ray emissivity is given by

$$e_X^{\bullet}(E', z) = \frac{1}{4\pi} \int_z L_X^{\bullet}(E', \Delta t') f_{\bullet} \frac{d\mathcal{N}_h}{dz'} dz', \quad (32)$$

where $\mathcal{N}_h$ is the number density of atomic-cooling halos, $f_{\bullet}$ their fraction harboring DCBHs, $\Delta t'$ the time interval between redshifts z and z'. We take the time-dependent $L_X^{\bullet}$ of a DCBH with initial mass 2×10^5 $M_{\odot}$ from Pacucci et al. (2015a)'s numerical simulations. Since we are mainly interested in the XRB spectral shape, its amplitude is left as a free parameter. To express different XRB levels, we vary the parameter $f_{\bullet}$, which is also re-

lated to the accretion rate density by

$$\dot{\rho}_\bullet(z) = \int_z \dot{M}_\bullet(\Delta t') f_\bullet \frac{d\mathcal{N}_{\rm h}}{dz'} dz', \quad (33)$$

where $\dot{M}_\bullet(\Delta t')$ is the accretion rate onto a BH at a time interval $\Delta t'$ after its birth and taken from the numerical simulations in Pacucci et al. (2015a)[6]. There are large uncertainties on the accretion rate density $\dot{\rho}_\bullet$, because both the occupation fraction of DCBHs in atomic-cooling halos and the BH mass distribution are not well-known. In the following, we therefore consider $\dot{\rho}_\bullet$ as a free parameter. The specific intensity of XRB at redshift z is then

$$J_X^\bullet(E,z) = (1+z)^3 \int_z e_X^\bullet(E',z') e^{-\tau_{\rm IGM}(E')} \frac{dr_p}{dz'} dz', \quad (34)$$

where $E' = E(1+z')/(1+z)$, and r_p is the proper distance. The IGM optical depth for X-ray photons is

$$\tau_{\rm IGM}(E') = \int_z^{z'} \left[\sum_{i={\rm H,He}} \bar{n}_i(z'') \sigma_i(E'') \right] \frac{dr_p}{dz''} dz'', \quad (35)$$

where$E'' = E(1+z'')/(1+z)$ and $\bar{n}_i$ is the mean number density of species i in the IGM (the trace amount metals in the IGM are ignored).

We plot the XRBs at $z = 13$ for the three types of source DCBH spectra in Fig. 6 for $\dot{\rho}_\bullet = 10^{-3}\ M_\odot {\rm yr}^{-1}{\rm Mpc}^{-3}$. From the fact that the present-day intensity does not fall below the redshifted intensity from the past, i.e.,

$$J_X(E, z=0) \gtrsim (1+z)^{-3} J_X(E(1+z), z), \quad (36)$$

we can put a constraint on the XRB at high redshift from the present-day XRB from unresolved sources, $EJ_X(1.5\ {\rm keV}, z=0) = 2\times10^{-13}$ erg s^{-1}cm^{-2}deg^{-2} (Moretti et al. 2012). The upper limit thus obtained for XRB at $z = 13$, $J(21\ {\rm keV}, z=13) < 1.2\times10^{-6}$ erg s^{-1}cm^{-2}keV^{-1}sr^{-1}, which is shown in Fig. 6 by a downward arrow.

Armed with the XRB spectrum above, we next investigate the impact of XRB on the DCBH formation. By repeating the temperature evolution calculations for one of the three DCBH spectra (BH1-3 with $N_{\rm H} = 1.3\times10^{25}, 8.0\times10^{24}$, and 5.0×10^{24}cm^{-2}) with the XRB of the same $N_{\rm H}$, we can derive the critical intensity $J_{\rm LW}^{\rm crit}$ for the DCBH formation as a function of $\dot{\rho}_\bullet$. The result is shown in Fig. 7 for the three DCBH spectra. For the same XRB level (i.e., $\dot{\rho}_\bullet$), the $J_{\rm LW}^{\rm crit}$ increases with decreasing $N_{\rm H}$ as in the cases without the XRB. In the case of BH1, $J_{\rm LW}^{\rm crit}$ remains ≈ 22 below $\dot{\rho}_\bullet \sim 10^{-4}\ M_\odot {\rm yr}^{-1}{\rm Mpc}^{-3}$. The behavior of $J_{\rm LW}^{\rm crit}$ is similar also for BH2(3) cases: $J_{\rm LW}^{\rm crit}$ is always ≈ 35 (54) below $\dot{\rho}_\bullet \sim 10^{-5}(10^{-6})\ M_\odot {\rm yr}^{-1}{\rm Mpc}^{-3}$.

[6] Strictly speaking, BHs with different initial masses have different growth histories. Although during the growth $L_X^\bullet$ is found to be almost proportional to the BH mass in Pacucci et al. (2015a) simulations, the final XRB may depend on both the number fraction of BHs in newly-formed atomic-cooling halos and the initial mass function of BHs.

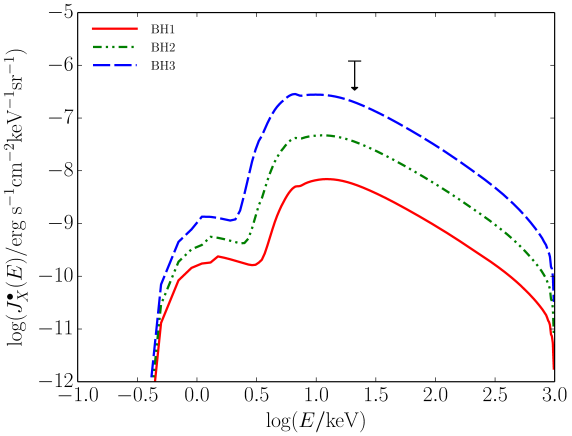

FIG. 6.— The spectral energy distributions of the X-ray background from DCBH populations with shielding columns $N_{\rm H} = 1.3\times10^{25}$ cm^{-2} ("BH1"), 8.0×10^{24} cm^{-2} ("BH2") and 5.0×10^{24} cm^{-2} ("BH3") from the bottom to top, respectively, assuming the BH accretion rate density $\dot{\rho}_\bullet = 1\times10^{-3} M_\odot {\rm yr}^{-1}{\rm Mpc}^{-3}$ at $z = 13$. The arrow is the upper limit derived from the present-day observed XRB level at 1.5 keV by Moretti et al. (2012)

Assuming that active DCBHs accrete at the Eddington limited rate[7] with radiative efficiency of 0.1, we can translate the accretion rate density $\dot{\rho}_\bullet$ into an *active* BH mass density $\rho_\bullet$:

$$\frac{\rho_\bullet}{M_\odot\ {\rm Mpc}^{-3}} \approx 4.1\times10^7 \frac{\dot{\rho}_\bullet}{M_\odot\ {\rm yr}^{-1}\ {\rm Mpc}^{-3}}. \quad (37)$$

Therefore, the critical active BH mass densities above which the XRB gives negative feedback for the DCBH formation are about $4\times10^3\ M_\odot{\rm Mpc}^{-3}$, $4\times10^2\ M_\odot{\rm Mpc}^{-3}$ and $4\times10^1\ M_\odot{\rm Mpc}^{-3}$ for the three $N_{\rm H}$ models, respectively.

With an accretion rate density $\dot{\rho}_\bullet$ higher than the above value, the XRB effect becomes noticeable and $J_{\rm LW}^{\rm crit}$ increases with $\dot{\rho}_\bullet$. However, even with $\dot{\rho}_\bullet$ as high as the maximum allowed by the present-day XRB level, the DCBH can still form with feasible $J_{\rm LW}^{\rm crit}$. For the BH1 model, the maximum allowed accretion rate density is $\approx 0.22\ M_\odot{\rm yr}^{-1}{\rm Mpc}^{-3}$, corresponding to $\rho_\bullet = 9.0\times10^6\ M_\odot{\rm Mpc}^{-3}$. At this limit $J_{\rm LW}^{\rm crit}$ only increases to ≈ 80. Under the same hypothesis, for the BH2(3) model at the maximally allowed accretion rate density, $\dot{\rho}_\bullet = 0.034(0.006)\ M_\odot{\rm yr}^{-1}{\rm Mpc}^{-3}$, we get $J_{\rm LW}^{\rm crit} \approx 170$ (390).

All these $J_{\rm LW}^{\rm crit}$ values are still much smaller than those for normal star-forming galaxies, i.e. $\sim 1000 - 10000$ (Sugimura et al. 2014; Latif et al. 2015; Agarwal et al. 2016b). This indicates that, even with the XRB, the DCBHs are efficient radiation sources for triggering DCBHs in nearby halos. Moreover, an accreting BH is usually much brighter than a galaxy, e.g. for a DCBH with mass $10^6\ M_\odot$, the Eddington luminosity is $\approx 1.3\times10^{44}$ erg s^{-1}, while a galaxy with our GAL spectrum and 10 $M_\odot{\rm yr}^{-1}$ has bolometric luminosity $\approx 3\times10^{42}$ erg s^{-1}. Hence, even if $J_{\rm LW}^{\rm crit}$ is the

[7] Note, however, that simulations by Pacucci et al. 2015a show that super-Eddington accretion may occur in highly-obscured environments, where radiation trapping is so efficient that photons are advected inward rather than being radiated away: thus, the effect of radiation pressure is dramatically reduced.

same, a BH radiation can exceeds $J_{\rm LW}^{\rm crit}$ more easily and can suppress H_2 formation in a larger number of nearby metal-free halos (Yue et al. 2014). Furthermore, if a star-forming galaxy is the dissociation radiation source, it also produces strong soft X-rays, which would counteract the H_2 dissociation (see Sec. 3.3.2 below). However it does not happen for the surrounded DCBHs since soft X-ray photons do not leak out from the envelope during the Compton-thick stage (~ 100 Myr).

Finally, we evaluate the appropriate distance from a halo to bear DCBH ("hatching halo") to the radiation source ("source halo"). If the hatching halo is close enough to the source, the radiation intensity exceeds $J_{\rm LW}^{\rm crit}$ and H_2 formation is suppressed. However, if the distance among them is too small, the hatching halo could by tidally disrupted by gravity of the source halo. The tidal radius of the hatching halo is defined as (Binney & Tremaine 1987; Chon et al. 2016)

$$r_{\rm TD} = \left(\frac{M_{\rm hat}}{3M_{\rm sou}}\right)^{1/3} d, \tag{38}$$

where $M_{\rm hat}$ and $M_{\rm sou}$ are the masses of the hatching halo and source halos, respectively, and d the distance among them. The matter of the hatching halo outside the tidal radius would be removed by the tidal force.

We conservatively require that for the hatching halo to keep its density without tidally disrupted, the tidal radius $r_{\rm TD}$ be larger than the virial radius $r_{\rm vir}$. Assuming $M_{\rm hat} \approx M_{\rm sou}$, we obtain $d > \sqrt[3]{3} r_{\rm vir} = 1.44 r_{\rm vir}$. In Fig. 7, we indicate the regions where the XRB from DCBHs is well below the present-day XRB constraints and the required $J_{\rm LW}^{\rm crit}$ can be provided by a source DCBH of 2×10^5 or 1×10^6 $M_\odot$ locating at the distance larger than $d > 1.44 r_{\rm vir}$, where $r_{\rm vir}$ is evaluated for $T_{\rm vir} = 10^4$K and $z = 13$. Fig. 7 indicates that, for any DCBH spectrum considered, there is still a large parameter space for the DCBH formation without being tidally disrupted.

3.3.2. *X-rays both from the first galaxies and DCBHs*

Next, we also consider the XRB created by the first galaxies $J_X^{\rm gal}$ and add it to that by DCBHs $J_X^\bullet$.

We assume the high-mass X-ray binaries (HMXBs) as the sources of XRB since they contribute most to the galactic X-ray radiation among three major contributors, i.e., HMXBs, low-mass X-ray binaries and hot interstellar medium (see e.g. Pacucci et al. 2014 for details). The X-ray SED of HMXBs follows the power law with index α_X, with its normalization depending on the SFR:

$$L_X^{\rm HMXB}(E) = \frac{(1-\alpha_X) L_{\rm band}({\rm SFR}, z)}{E_2^{(1-\alpha_X)} - E_1^{(1-\alpha_X)}} E^{-\alpha_X}, \tag{39}$$

where $L_{\rm band}$ is the X-ray luminosity in the energy range considered ($E_1 < E < E_2$) and we adopt the spectral index $\alpha_X = 1.5$ in the following. We use the fitting formula for the luminosity in 2 - 10 keV (below 2 keV the X-ray photons might be absorbed by host galaxy gas, therefore the above normalization would be not valid, see Pacucci et al. 2014) by Basu-Zych et al. (2013)

$$\log\left(\frac{L_{\rm band}}{\rm erg\ s^{-1}}\right) = 0.97\log(1+z) + 0.65\log\left(0.67\frac{\rm SFR}{\rm M_\odot yr^{-1}}\right) + 39.80, \tag{40}$$

and to model the scatter we assume a 0.5 dex variance for this relation. Although the almost linear dependence on redshift, $L_{\rm band} \propto (1+z)^{0.97}$, is obtained from fitting to $z < 4$ samples, we here extrapolate it to galaxies at higher redshifts. We have multiplied the SFR by a factor 0.67 (Madau & Dickinson 2014) so that here the SFR corresponds to Salpeter IMF with mass limits of 0.1 and 100 $M_\odot$, we adopted. At $z = 13$ and SFR$= 1$ $M_\odot {\rm yr}^{-1}$, Eq. (40) gives $\log(L_{\rm band}) = 40.8^{+0.5}_{-0.5}$. Note that this brackets the fiducial value 40.5 adopted in Furlanetto (2006).

The SFR is assumed proportional to halo mass growth rate:

$${\rm SFR}(M, z) = f_* \frac{\Omega_b}{\Omega_m} \frac{M}{2\Delta t_{\rm SF}(M, z)}, \tag{41}$$

where M is the halo mass, and the star formation time scale, $\Delta t_{\rm SF}$, is the time since the median formation time, which is defined as the time when the halo has collected half of its mass, to the considering redshift z (Giocoli et al. 2007), and f_* is the star formation efficiency.

The star formation efficiency f_* is calibrated from the observed UV luminosity density $\rho_{\rm UV}$, which is derived from the UV luminosity functions of high-z galaxies. By extrapolating the luminosity function in Bouwens et al. (2015b) down to the absolute UV magnitude -10, Bouwens et al. (2015a) has obtained $\rho_{\rm UV}$ as a function of redshift and it is $\rho_{\rm UV} = 10^{26.2\pm0.2}$ erg s^{-1}Hz^{-1} Mpc^{-3} at $z = 10$. By equating this with the sum of contributions from all halos calculated theoretically:

$$\rho_{\rm UV} = \int_{M_{\rm min}} l_{\rm UV}(\Delta t_{\rm SF}) {\rm SFR}(M, z) \frac{d\mathcal{N}}{dM} dM, \tag{42}$$

where $M_{\rm min}$ is the minimum halo mass that can form stars and for which we adopt the virial mass of $T_{\rm vir} = 10^4$ K, $d\mathcal{N}/dM$ is the halo mass function (Sheth & Tormen 1999; Sheth et al. 2001) and $l_{\rm UV}$ is the UV (at 1500 Å) luminosity per unit SFR for continuous star formation mode with Salpeter IMF (0.1 - 100 $M_\odot$) and metallicity $Z = 0.02$ $Z_\odot$, taken from `STARBURST99`. We then obtain $f_* = 0.022^{+0.012}_{-0.008}$.

The XRB from first galaxies at redshift z can be calculated by

$$J_X^{\rm gal}(E, z) = (1+z)^3 \int_z e_X^{\rm gal}(E', z') {\rm e}^{-\tau_{\rm IGM}(E')} \frac{dr_{\rm p}}{dz'} dz', \tag{43}$$

where the X-ray emissivity

$$e_X^{\rm gal}(E', z) = \frac{1}{4\pi} \int_{M_{\rm min}} f_{\rm esc,X}(E') L_{\rm X}^{\rm HMXB}(E') \frac{d\mathcal{N}}{dM} dM. \tag{44}$$

The X-ray escape fraction $f_{\rm esc,X}$ depends on the neutral hydrogen, neutral helium and metal content of host

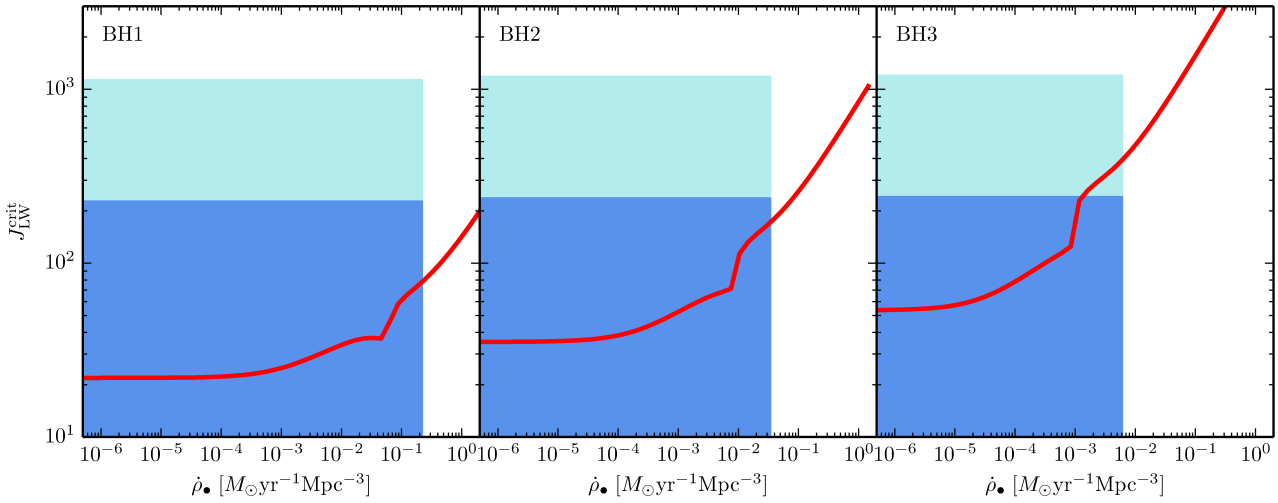

FIG. 7.— $J_{\rm LW}^{\rm crit}$ as a function of $\dot{\rho}_\bullet$ for three DCBH models. We fill the regions where the XRB produced by $\dot{\rho}_\bullet$ is below the present-day XRB level constraints, and the required $J_{\rm LW}^{\rm crit}$ can be provided by an emitting DCBH with mass 2×10^5 $M_\odot$ (dark shaded) and 1×10^6 $M_\odot$ (light & dark shaded).

galaxies,

$$f_{\rm esc,X}(E) = \exp\left[-(\sigma_{X,1}(E)N_{\rm HI}^{\rm gal} + \sigma_{X,2}(E)ZN_{\rm HI}^{\rm gal})\right], \quad (45)$$

where $N_{\rm HI}^{\rm gal}$ is the column number density of neutral hydrogen, $\sigma_{X,1}$ and $\sigma_{X,2}$ the synthesis photo-electric cross-section of neutral hydrogen and helium only, and of metal elements with Solar abundance, respectively Both $\sigma_{X,1}$ and $\sigma_{X,2}$ have been converted to those in units per hydrogen atom (Balucinska-Church & McCammon 1992).

The neutral hydrogen column density in first galaxies is largely unknown. Lehmer et al. (2016) provide z-dependent expressions for the X-ray luminosity in both 0.5 - 2 keV and 2 - 10 keV bands. By assuming that the 2 - 10 keV luminosity approximates the intrinsic one, while that of 0.5 - 2 keV is attenuated one, and comparing these two, we derive $N_{\rm HI}^{\rm gal} \sim 3\times10^{21}$ - 3×10^{22} cm^{-2} for SFR $\sim 10^{-3}$ - 50 $M_\odot{\rm yr}^{-1}$ at $z = 13$. Although such value should be only considered as an educated guess, we nevertheless assume a fiducial value $\log N_{\rm HI}^{\rm gal} = 22$ with ±0.5 dex scatter, and use it for all $z \geq 13$.

In Fig. 8, we show the XRB from first galaxies at $z = 13$ with the variance. They contribute $\sim 0.3\% - 6\%$ to the unresolved present-day XRB at 1.5 keV. The total XRB is the sum of $J_X^{\rm gal}$ and the DCBH contribution $J_X^\bullet$. Recall that the latter is a function of $\dot{\rho}_\bullet$. For this XRB, we re-calculate $J_{\rm LW}^{\rm crit}$ for each $\dot{\rho}_\bullet$. The results are plotted in Fig. 9. Comparing with the values with DCBH XRB only, the $J_{\rm LW}^{\rm crit}$ is boosted by about factors of 2 - 20. This indicates that the XRB from first galaxies may have significant negative influence on the DCBH formation although DCBH formation is still feasible.

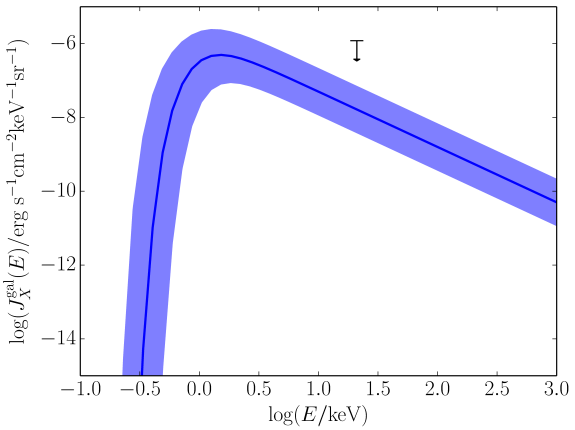

FIG. 8.— The $z = 13$ XRB from first galaxies. Fiducial model with $f_* = 0.022$, $\log N_{\rm HI}^{\rm gal} = 22$ and $\log L_{\rm band} = 0.93\log(1+z) + 0.65\log(0.67\times{\rm SFR}) + 39.80$ is plotted by solid line. The variance corresponding to $f_* = 0.022^{+0.012}_{-0.008}$, $\log N_{\rm HI} = 22^{+0.5}_{-0.5}$ and $\log L_{\rm band} = 0.93\log(1+z) + 0.65\log(0.67\times{\rm SFR}) + 39.80 \pm 0.5$ is shown with a shaded region.

4. CONCLUSIONS AND DISCUSSION

We have investigated the critical specific intensity of the DCBH radiation that could suppress H_2 formation and cooling in a nearby collapsing gas cloud by one-zone calculations. If the radiation from the emitting DCBH is higher than the critical intensity, we expect that a new DCBH forms in the gas cloud. We used three realistic DCBH SED models from numerical simulations with initial column number density for the absorbing envelope $N_{\rm H} = 1.3\times10^{25}$ cm^{-2}, $N_{\rm H} = 8.0\times10^{24}$ cm^{-2} and $N_{\rm H} = 5.0\times10^{24}$ cm^{-2}, respectively.

We have found that:

- DCBH spectra are very effective at photo-detaching H^-, a catalyst species for H_2 formation. Depending on the obscuring gas column density, the ratio between H^- photo-detachment and H_2 photo-dissociation rates for the DCBH with $N_{\rm H} = 1.3\times10^{25}$ cm^{-2} is $k^{\rm BH1}_{\rm H^-,det}/k^{\rm BH1}_{\rm H_2,dis} = 4.1\times10^4$, i.e. comparable to that of a blackbody spectrum with effective temperature 10^4 K which is $k^{\rm BB}_{\rm H^-,det}/k^{\rm BB}_{\rm H_2,dis} = 7.2\times10^4$. For the other two DCBH SEDs the $k^{\rm BH2}_{\rm H^-,det}/k^{\rm BH2}_{\rm H_2,dis} = 1.4\times10^4$ and $k^{\rm BH3}_{\rm H^-,det}/k^{\rm BH3}_{\rm H_2,dis} = 4.8\times10^3$, still much higher than

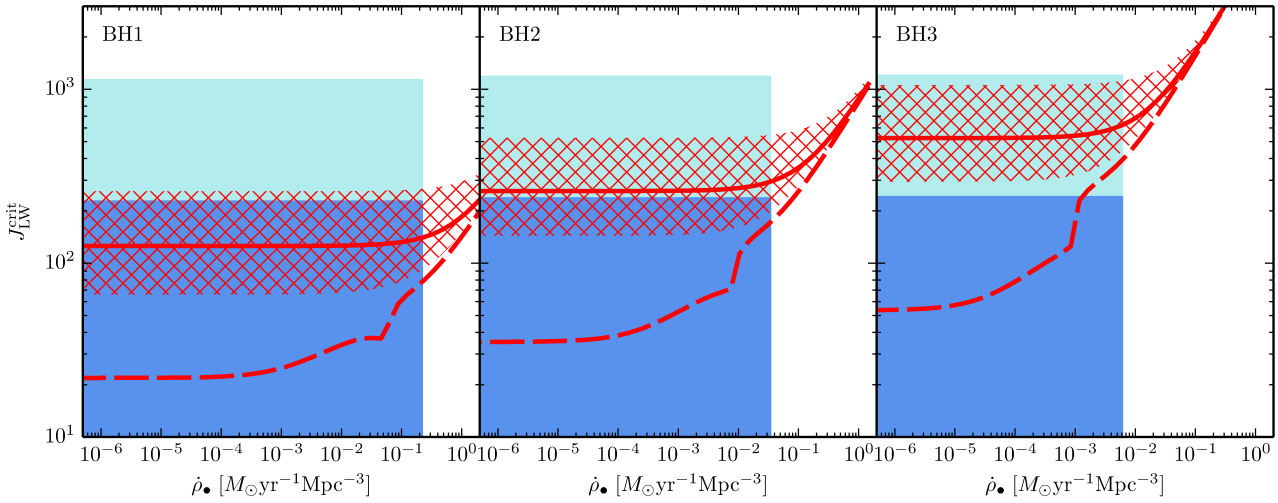

FIG. 9.— The $J_{\rm LW}^{\rm crit}$ against $\dot{\rho}_\bullet$, XRB from first galaxies is included as well. The shaded regions are allowed space by present-day XRB constraints and gravitationally disruption, see Fig. 7. Solid curves correspond to fiducial parameters of first galaxies in Fig. 8 while hatched regions are variance. For reference we also plot the $J_{\rm LW}^{\rm crit}$ curves in the absence of XRB from first galaxies by dashed lines.

a typical star-forming galaxy which only yields $k_{\rm H^-,det}^{\rm GAL}/k_{\rm H_2,dis}^{\rm GAL} = 44$.

- Ignoring the effect of X-rays, the critical field intensity to suppress H_2 formation for the three DCBH SEDs is $J_{\rm LW}^{\rm crit} \approx 22$, 35 and 54, respectively. Note that this is similar to a blackbody radiation field with effective temperature 10^4 K, ($J_{21}^{\rm crit} \approx 30$), but much lower than for a typical star-forming galaxy spectrum ($J_{\rm LW}^{\rm crit} \approx 700$). Hence, an emitting DCBH can trigger the formation of DCBH in a nearby collapsing gas cloud much more efficiently than galaxies.

- If an X-ray background (XRB) produced by previously formed DCBH is present, it may promote H_2 formation and increase $J_{\rm LW}^{\rm crit}$. For the $N_{\rm H} = 1.3\times10^{25}$ cm^{-2} model, if the accretion rate density is $\dot{\rho}_\bullet \lesssim 10^{-4}$ $M_\odot$yr^{-1}Mpc^{-3}, XRB plays a negligible role. However, even if $\dot{\rho}_\bullet$ reaches the maximum value allowed by the present-day XRB level, i.e. ~ 0.22 $M_\odot$ yr^{-1}Mpc^{-3}, $J_{\rm LW}^{\rm crit}$ only increases to $\approx$ 80. For the $N_{\rm H} = 8.0(5.0)\times10^{24}$ cm^{-2} SED models, XRB effect is negligible when $\dot{\rho}_\bullet \lesssim 10^{-5}(10^{-6})$ $M_\odot$yr^{-1}Mpc^{-3}, and the $J_{\rm LW}^{\rm crit}$ increases to $\approx$ 170(390) at the maximum $\dot{\rho}_\bullet$ allowed by the present-day XRB level, which is $\approx$ 0.034(0.006) $M_\odot$ yr^{-1}Mpc^{-3}. However, if the additional but uncertain XRB contribution from first galaxies is included, it may modify the result by factors in the range 2 - 20.

Finally, it is worth noting that several works, for instance Shang et al. (2010), Latif et al. (2014) and Latif et al. (2015), have shown that the $J_{\rm LW}^{\rm crit}$ derived from 3D simulations is almost $\sim 10-100$ times higher than from one-zone calculations, "*due to the inability of one-zone models to simulate shocks, collapse dynamics and hydrodynamical effects*" (Latif et al. 2015). Moreover, they also found that the $J_{\rm LW}^{\rm crit}$ varies from halo to halo. Under these circumstances, we might be significantly underestimating $J_{\rm LW}^{\rm crit}$. Further numerical work will be necessary to clarify this point.

BY is supported by the CAS Pioneer Hundred Talents (Young Talents) Program. FP acknowledges the NASA-ADAP grant MA160009.

REFERENCES

Abel, T., Anninos, P., Zhang, Y., & Norman, M. L. 1997, New A, 2, 181, astro-ph/9608040
Abgrall, H., Le Bourlot, J., Pineau Des Forets, G., Roueff, E., Flower, D. R., & Heck, L. 1992, A&A, 253, 525
Abgrall, H., & Roueff, E. 1989, A&AS, 79, 313
Agarwal, B., Dalla Vecchia, C., Johnson, J. L., Khochfar, S., & Paardekooper, J.-P. 2014, MNRAS, 443, 648, 1403.5267
Agarwal, B., Davis, A. J., Khochfar, S., Natarajan, P., & Dunlop, J. S. 2013, MNRAS, 432, 3438, 1302.6996
Agarwal, B., Johnson, J. L., Zackrisson, E., Labbe, I., van den Bosch, F. C., Natarajan, P., & Khochfar, S. 2016a, MNRAS, 460, 4003, 1510.01733
Agarwal, B., Khochfar, S., Johnson, J. L., Neistein, E., Dalla Vecchia, C., & Livio, M. 2012, MNRAS, 425, 2854, 1205.6464
Agarwal, B., Smith, B., Glover, S., Natarajan, P., & Khochfar, S. 2016b, MNRAS, 459, 4209, 1504.04042
Alvarez, M. A., Wise, J. H., & Abel, T. 2009, ApJ, 701, L133, 0811.0820
Aykutalp, A., Wise, J. H., Spaans, M., & Meijerink, R. 2014, ApJ, 797, 139, 1409.0543
Balucinska-Church, M., & McCammon, D. 1992, ApJ, 400, 699
Barkana, R., & Loeb, A. 2001, Phys. Rep., 349, 125, arXiv:astro-ph/0010468
Basu-Zych, A. R. et al. 2013, ApJ, 762, 45, 1210.3357
Begelman, M. C. 2010, MNRAS, 402, 673, 0910.4398
Begelman, M. C., Rossi, E. M., & Armitage, P. J. 2008, MNRAS, 387, 1649, 0711.4078
Begelman, M. C., Volonteri, M., & Rees, M. J. 2006, MNRAS, 370, 289, astro-ph/0602363
Binney, J., & Tremaine, S. 1987, Galactic dynamics
Bouwens, R. J., Illingworth, G. D., Oesch, P. A., Caruana, J., Holwerda, B., Smit, R., & Wilkins, S. 2015a, ApJ, 811, 140, 1503.08228
Bouwens, R. J. et al. 2015b, ApJ, 803, 34, 1403.4295
Bowler, R. A. A., McLure, R. J., Dunlop, J. S., McLeod, D. J., Stanway, E. R., Eldridge, J. J., & Jarvis, M. J. 2016, ArXiv e-prints, 1609.00727
Bromm, V., Coppi, P. S., & Larson, R. B. 2002, ApJ, 564, 23, arXiv:astro-ph/0102503

Bromm, V., & Loeb, A. 2003, ApJ, 596, 34, arXiv:astro-ph/0212400
Choi, J.-H., Shlosman, I., & Begelman, M. C. 2015, MNRAS, 450, 4411, 1412.2761
Chon, S., Hirano, S., Hosokawa, T., & Yoshida, N. 2016, ArXiv e-prints, 1603.08923
Dijkstra, M., Ferrara, A., & Mesinger, A. 2014, MNRAS, 442, 2036, 1405.6743
Dijkstra, M., Haiman, Z., Mesinger, A., & Wyithe, J. S. B. 2008, MNRAS, 391, 1961, 0810.0014
Eisenstein, D. J., & Hu, W. 1998, ApJ, 496, 605, arXiv:astro-ph/9709112
Fan, X. et al. 2003, AJ, 125, 1649, astro-ph/0301135
Ferrara, A., Salvadori, S., Yue, B., & Schleicher, D. 2014, MNRAS, 443, 2410, 1406.6685
Furlanetto, S. R. 2006, MNRAS, 371, 867, astro-ph/0604040
Galli, D., & Palla, F. 1998, A&A, 335, 403, arXiv:astro-ph/9803315
Giocoli, C., Moreno, J., Sheth, R. K., & Tormen, G. 2007, MNRAS, 376, 977, astro-ph/0611221
Glover, S. C. O. 2015, MNRAS, 451, 2082, 1501.05960
——. 2016, ArXiv e-prints, 1610.05679
Glover, S. C. O., & Abel, T. 2008, MNRAS, 388, 1627, 0803.1768
Glover, S. C. O., & Brand, P. W. J. L. 2001, MNRAS, 321, 385, arXiv:astro-ph/0005576
Glover, S. C. O., & Jappsen, A. 2007, ApJ, 666, 1, 0705.0182
Habouzit, M., Volonteri, M., Latif, M., Dubois, Y., & Peirani, S. 2016, MNRAS, 1601.00557
Heger, A., Fryer, C. L., Woosley, S. E., Langer, N., & Hartmann, D. H. 2003, ApJ, 591, 288, astro-ph/0212469
Hirata, C. M., & Padmanabhan, N. 2006, MNRAS, 372, 1175, astro-ph/0606437
Hollenbach, D., & McKee, C. F. 1979, ApJS, 41, 555
Hosokawa, T., Omukai, K., Yoshida, N., & Yorke, H. W. 2011, Science, 334, 1250, 1111.3649
Inayoshi, K., & Omukai, K. 2011, MNRAS, 416, 2748, 1106.2812
Inayoshi, K., Omukai, K., & Tasker, E. 2014, MNRAS, 445, L109, 1404.4630
Inayoshi, K., & Tanaka, T. L. 2015, MNRAS, 450, 4350, 1411.2590
Jeon, M., Pawlik, A. H., Greif, T. H., Glover, S. C. O., Bromm, V., Milosavljević, M., & Klessen, R. S. 2012, ApJ, 754, 34, 1111.6305
Jiang, L., Fan, X., Vestergaard, M., Kurk, J. D., Walter, F., Kelly, B. C., & Strauss, M. A. 2007, AJ, 134, 1150, 0707.1663
Johnson, J. L., Whalen, D. J., Agarwal, B., Paardekooper, J.-P., & Khochfar, S. 2014, MNRAS, 445, 686, 1405.2081
Johnson, J. L., Whalen, D. J., Li, H., & Holz, D. E. 2013, ApJ, 771, 116, 1211.0548
Koushiappas, S. M., Bullock, J. S., & Dekel, A. 2004, MNRAS, 354, 292, astro-ph/0311487
Kurk, J. D. et al. 2007, ApJ, 669, 32, 0707.1662
Latif, M. A., Bovino, S., Grassi, T., Schleicher, D. R. G., & Spaans, M. 2015, MNRAS, 446, 3163, 1408.3061
Latif, M. A., Bovino, S., Van Borm, C., Grassi, T., Schleicher, D. R. G., & Spaans, M. 2014, MNRAS, 443, 1979, 1404.5773
Latif, M. A., & Ferrara, A. 2016, ArXiv e-prints, 1605.07391
Latif, M. A., Schleicher, D. R. G., & Hartwig, T. 2016, MNRAS, 458, 233, 1510.02788
Latif, M. A., Schleicher, D. R. G., Schmidt, W., & Niemeyer, J. 2013a, MNRAS, 433, 1607, 1304.0962
Latif, M. A., Schleicher, D. R. G., Schmidt, W., & Niemeyer, J. C. 2013b, MNRAS, 436, 2989, 1309.1097
Lehmer, B. D. et al. 2016, ApJ, 825, 7, 1604.06461
Leitherer, C., Ortiz Otálvaro, P. A., Bresolin, F., Kudritzki, R.-P., Lo Faro, B., Pauldrach, A. W. A., Pettini, M., & Rix, S. A. 2010, ApJS, 189, 309, 1006.5624
Leitherer, C. et al. 1999, ApJS, 123, 3, astro-ph/9902334
Lepp, S., & Shull, J. M. 1984, ApJ, 280, 465
Lodato, G., & Natarajan, P. 2006, MNRAS, 371, 1813, astro-ph/0606159
Madau, P., & Dickinson, M. 2014, ARA&A, 52, 415, 1403.0007
Martin, P. G., Schwarz, D. H., & Mandy, M. E. 1996, ApJ, 461, 265
Maselli, A., Ferrara, A., & Ciardi, B. 2003, MNRAS, 345, 379, arXiv:astro-ph/0307117
Moretti, A., Vattakunnel, S., Tozzi, P., Salvaterra, R., Severgnini, P., Fugazza, D., Haardt, F., & Gilli, R. 2012, A&A, 548, A87, 1210.6377
Morganson, E. et al. 2012, AJ, 143, 142, 1109.6241
Mortlock, D. J. et al. 2011, Nature, 474, 616, 1106.6088
Omukai, K. 2000, ApJ, 534, 809, arXiv:astro-ph/0003212
——. 2001, ApJ, 546, 635, arXiv:astro-ph/0011446
Omukai, K., Hosokawa, T., & Yoshida, N. 2010, ApJ, 722, 1793, 1008.4262
Omukai, K., & Nishi, R. 1998, ApJ, 508, 141, astro-ph/9811308
Omukai, K., Tsuribe, T., Schneider, R., & Ferrara, A. 2005, ApJ, 626, 627, astro-ph/0503010
Pacucci, F., & Ferrara, A. 2015, MNRAS, 448, 104, 1501.00989
Pacucci, F., Ferrara, A., Grazian, A., Fiore, F., Giallongo, E., & Puccetti, S. 2016, MNRAS, 459, 1432, 1603.08522
Pacucci, F., Ferrara, A., Volonteri, M., & Dubus, G. 2015a, MNRAS, 454, 3771, 1506.05299
Pacucci, F., Mesinger, A., Mineo, S., & Ferrara, A. 2014, MNRAS, 443, 678, 1403.6125
Pacucci, F., Volonteri, M., & Ferrara, A. 2015b, MNRAS, 452, 1922, 1506.04750
Palla, F., Salpeter, E. E., & Stahler, S. W. 1983, ApJ, 271, 632
Pallottini, A. et al. 2015, MNRAS, 453, 2465, 1506.07173
Planck Collaboration et al. 2015, ArXiv e-prints, 1502.01589
Regan, J. A., & Haehnelt, M. G. 2009, MNRAS, 396, 343, 0810.2802
Regan, J. A., Johansson, P. H., & Wise, J. H. 2014, ApJ, 795, 137, 1407.4472
——. 2016, MNRAS, 461, 111, 1603.06612
Shang, C., Bryan, G. L., & Haiman, Z. 2010, MNRAS, 402, 1249, 0906.4773
Shapiro, P. R., & Kang, H. 1987, ApJ, 318, 32
Sheth, R. K., Mo, H. J., & Tormen, G. 2001, MNRAS, 323, 1, astro-ph/9907024
Sheth, R. K., & Tormen, G. 1999, MNRAS, 308, 119, arXiv:astro-ph/9901122
Shull, J. M., & van Steenberg, M. E. 1985, ApJ, 298, 268
Smidt, J., Wiggins, B. K., & Johnson, J. L. 2016, ApJ, 829, L6, 1603.00888
Smith, A., Bromm, V., & Loeb, A. 2016, MNRAS, 460, 3143, 1602.07639
Sobral, D., Matthee, J., Darvish, B., Schaerer, D., Mobasher, B., Röttgering, H. J. A., Santos, S., & Hemmati, S. 2015, ApJ, 808, 139, 1504.01734
Stacy, A., & Bromm, V. 2007, MNRAS, 382, 229, 0705.3634
Stecher, T. P., & Williams, D. A. 1967, ApJ, 149, L29
Sugimura, K., Omukai, K., & Inoue, A. K. 2014, MNRAS, 445, 544, 1407.4039
Tanaka, T., Perna, R., & Haiman, Z. 2012, MNRAS, 425, 2974, 1205.6467
Umeda, H., Hosokawa, T., Omukai, K., & Yoshida, N. 2016, ApJ, 830, L34, 1609.04457
Valdés, M., & Ferrara, A. 2008, MNRAS, 387, L8, 0803.0370
Valiante, R., Schneider, R., Volonteri, M., & Omukai, K. 2016, MNRAS, 457, 3356, 1601.07915
Vázquez, G. A., & Leitherer, C. 2005, ApJ, 621, 695, astro-ph/0412491
Venemans, B. P. et al. 2013, ApJ, 779, 24, 1311.3666
Visbal, E., Haiman, Z., Terrazas, B., Bryan, G. L., & Barkana, R. 2014, MNRAS, 445, 107, 1402.0882
Volonteri, M. 2010, A&A Rev., 18, 279, 1003.4404
Wolcott-Green, J., Haiman, Z., & Bryan, G. L. 2011, MNRAS, 418, 838, 1106.3523
——. 2016, ArXiv e-prints, 1609.02142
Wu, X.-B. et al. 2015, Nature, 518, 512, 1502.07418
Yoshida, N., Omukai, K., Hernquist, L., & Abel, T. 2006, ApJ, 652, 6, arXiv:astro-ph/0606106
Yue, B., Ferrara, A., Salvaterra, R., Xu, Y., & Chen, X. 2014, MNRAS, 440, 1263, 1402.5675

APPENDIX

A. THE OPTICAL DEPTHS FOR H_2, H^-, AND H_2^+

Here we check the validity of the optically thin assumption made for the H^- detachment radiation and for the H_2^+ dissociation radiation. For H^-, the mean optical depth of the gas cloud is

$$\left\langle \tau_{\mathrm{H}^-,\mathrm{det}} \right\rangle = \lambda_J/2 \left\langle \sigma_{\mathrm{H}^-,\mathrm{det}} \right\rangle n_{\mathrm{H}^-}, \tag{A1}$$

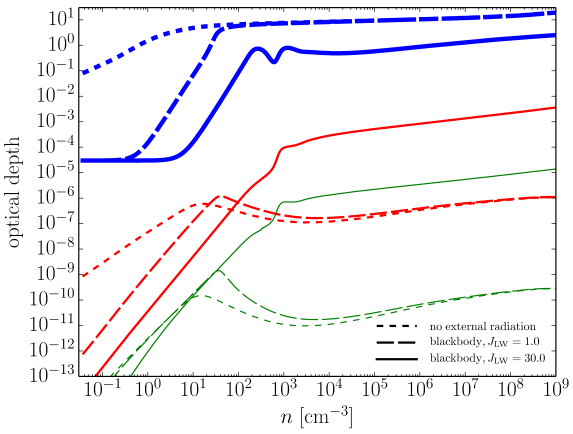

FIG. 10.— The optical depth against n, thick lines are $-\log(f_{\rm sh})$ for H_2 self-shielding, medium and thin lines are for the H^- and H_2^+ respectively.

where the mean cross-section is

$$\left\langle \sigma_{\rm H^-,det} \right\rangle = k_{\rm H^-,det} \left(\int_{\nu_{0.755}}^{\nu_{13.6}} \frac{4\pi J(\nu)}{h\nu} d\nu \right)^{-1}. \tag{A2}$$

This mean cross-section only depends on the spectral shape of the external radiation field, however is independent of its strength which appears in both numerator and denominator. For the BB spectrum, $\left\langle \sigma_{\rm H^-,det} \right\rangle = 2.8 \times 10^{-17}$ cm^2. Similarly, we can also calculate the mean cross-section for H_2^+, for which we get $\left\langle \sigma_{\rm H_2^+,dis} \right\rangle = 7.0 \times 10^{-19}$ cm^{-2}, and the corresponding mean optical depth $\left\langle \tau_{\rm H_2^+,dis} \right\rangle$.

In Fig. 10 we plot $\left\langle \tau_{\rm H^-,det} \right\rangle$, $\left\langle \tau_{\rm H_2^+,dis} \right\rangle$ and $-\log(f_{\rm sh})$ (considered as the mean optical depth to LW radiation) respectively against the n for different external radiation field strengths. This figure shows that, since the optical depth to H? detachment radiation and to H+2 dissociation radiation are always much smaller, it is then safe to ignore them. On the other hand, even when $J_{\rm LW} \gtrsim J_{\rm LW}^{\rm crit}$, at $n \gtrsim 10^3$ cm^{-3} the self-shielding effect to LW radiation is not negligible.

B. PARAMETER WINDOWS FOR ENHANCED DCBH FORMATION PROBABILITY

In our fiducial model we adopt the following initial setup: $z_{\rm ta} = 30.6$; adiabatic IGM temperature; ionization fraction 10^{-4}, H_2 fraction 10^{-6}. In this section we investigate the influence of alternative initial setups on DCBH formation.

We first check that for BH1 radiation field, using $z_{\rm ta} = 16$ while keeping other parameters fixed to the fiducial ones, we get $J_{\rm LW}^{\rm crit} \approx 20$. As for the fiducial setup for which we get $J_{\rm LW}^{\rm crit} \approx 22$, we conclude that DCBH formation is insensitive to cosmic epoch at which the process takes place.

We then take into account pre-heating of gas by X-rays and shocks before it collapses. In such case at $z = z_{\rm ta}$ the gas temperature is higher than the adiabatic IGM temperature. We set the initial gas temperature $T_0 = 30$, 50, 100 and 1000 K respectively, keeping other initial setups the same as our fiducial model, and find that $J_{\rm LW}^{\rm crit}$ increases with increasing T_0: $J_{\rm LW}^{\rm crit} \approx 39$, 49, 50 and 51 for $T_0 = 30$, 50, 100 and 1000 K respectively. When $T_0 \gtrsim 100$ K the $J_{\rm LW}^{\rm crit}$ almost does no longer increase. We conclude that ignoring the gas pre-heating may underestimate the critical field intensity by a factor at most ≈ 2.

Interestingly, we find that in the model with $T_0 = 30$ K, H_2 formation and cooling could also be suppressed even when the radiation field strength is smaller than $J_{\rm LW}^{\rm crit} \approx 39$, as long as it is in a narrow range $14.5 \lesssim J_{\rm LW} \lesssim 15.5$, as shown by Fig. 11 where we plot the gas temperature at the final step of our calculations ($n \sim 10^9$ cm^{-3}) against $J_{\rm LW}$. To investigate the physics behind this interesting phenomenon, we look through the evolution track and find that when $J_{\rm LW}$ is in this range, the gas almost simultaneously reaches the maximum temperature $\sim 10^4$ K and the critical density for H-H_2 collisional dissociation, $n_{\rm cr,H}$ (see Martin et al. 1996). When gas number density is higher than $n_{\rm cr,H}$, H_2 is dissociated via the $H_2 + H \xrightarrow{k_{13}} 3H$ reaction with reaction rate k_{13} approximately proportional to $\exp(-5 \times 10^4/T)$. It has strong temperature dependence hence the H_2 is dissociated very efficiently at the maximum gas temperature, resulting in suppressed H_2 cooling. If, however, the $J_{\rm LW}$ is smaller than $\sim$14.5, the gas cools earlier and never has a chance to reach the temperature $\sim 10^4$ K, and the collision dissociation is not efficient because of the low temperature; or if the $J_{\rm LW}$ is larger than $\sim$15.5, the radiation reduces (but not fully suppresses) H_2 cooling and the gas temperature reaches 10^4 K before the gas density reaches $n_{\rm cr,H}$, therefore the H_2 cannot be dissociated efficiently via H-H_2 collisions because of the low density, and then the gas temperature decreases soon. The same phenomenon also exists in the $T_0 = 50$ K model, except that the feasible field intensity range is even narrower. However, it does not exist in our fiducial model where $T_0 = 19.8$ K, and the model with $T_0 > 50$ K.

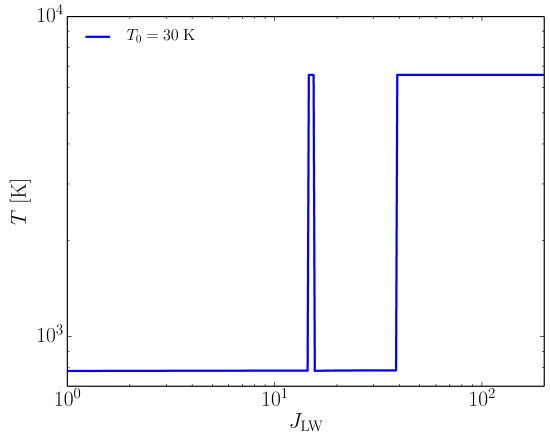

FIG. 11.— For BH1 radiation field, the gas temperature at $n \sim 10^9$ cm^{-3} vs. $J_{\rm LW}$ when gas has initial temperature $T_0 = 30$ K.

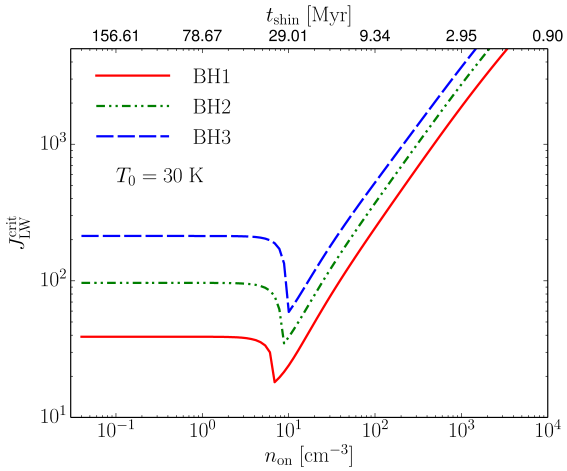

FIG. 12.— Same to Fig. 5 however $T_0 = 30$ K.

Although the physics mechanism is interesting, the above phenomenon may hardly occur in more realistic cases in which the strength of the external radiation varies with time. However, this mechanism could work in other situations and decrease the critical field intensity, see below.

We re-calculate the $J_{\rm LW}^{\rm crit}$ - $n_{\rm on}$ relation for $T_0 = 30$ K, the results are plotted in Fig. 12. We find the $J_{\rm LW}^{\rm crit}$ does not increase monotonically with $n_{\rm on}$. Instead, for BH1 (BH2, BH3) radiation field when 2 cm$^{-3} \lesssim n_{\rm on} \lesssim 15$ cm^{-3} (2 cm$^{-3} \lesssim n_{\rm on} \lesssim 25$ cm^{-3}, 2 cm$^{-3} \lesssim n_{\rm on} \lesssim 35$ cm^{-3}), $J_{\rm LW}^{\rm crit}$ is even smaller than models where the external radiation field irradiates the collapsing gas cloud longer. For example, if the external radiation is switched on at ~ 7 cm^{-3}, H_2 suppression is achieved with an intensity as low as $J_{\rm LW}^{\rm crit} \sim 18$ for BH1 radiation field. We clarify here that the $J_{\rm LW}^{\rm crit}$ is not the left boundary of the narrow peak in Fig. 11, instead it is the left boundary of the plateau, i.e. for all $J_{\rm LW} \geq J_{\rm LW}^{\rm crit}$ the H_2 formation and cooling will be suppressed.

The physics of this phenomenon is same to the above. Given $J_{\rm LW} = 30$, in Fig. 13 we plot the the temperature tracks for $n_{\rm on} = (1, 10, 20)$ cm^{-3}. We also plot the T-$n_{\rm cr,H}$ curve in the same panel. Note that $J_{\rm LW} = 30$ is smaller than the $J_{\rm LW}^{\rm crit}$ for $n_{\rm on} = 1$ and 20 cm^{-3}, but larger than the $J_{\rm LW}^{\rm crit}$ for $n_{\rm on} = 10$ cm^{-3}. As seen from Fig. 13, for $n_{\rm on} = 1$ cm^{-3} and 20 cm^{-3} cases, the temperature track and the T-$n_{\rm cr,H}$ curve intersect at $T \sim 500$ K. However for the $n_{\rm on} = 10$ cm^{-3} case, the intersection is near 10000 K. Recall that at $\gtrsim n_{\rm cr,H}$ the reaction rate k_{13} approximately proportional to $\exp(-5 \times 10^4/T)$. Hence, only if the temperature track and the T-$n_{\rm cr,H}$ curve intersect at high temperatures the H_2 can be rapidly dissociated by H-H_2 collisions, see the colored segment of each curve where the k_{13} is shown. In such a situation the H_2 formation and cooling suppression by a weaker external radiation is possible. Moreover, when $n_{\rm on} \gtrsim 100$ cm^{-3}, the $J_{\rm LW}^{\rm crit}$ increases rapidly because otherwise the previously formed H_2 has already cooled the gas to a low temperatures. We note that from $n \sim 2$ cm^{-3} to ~ 15 cm^{-3} only about ~ 35 Myr time elapses. It is still a short time-scale opportunity for DCBH to form in a weaker external radiation field.

C. REACTION RATES AND COOLING FUNCTIONS

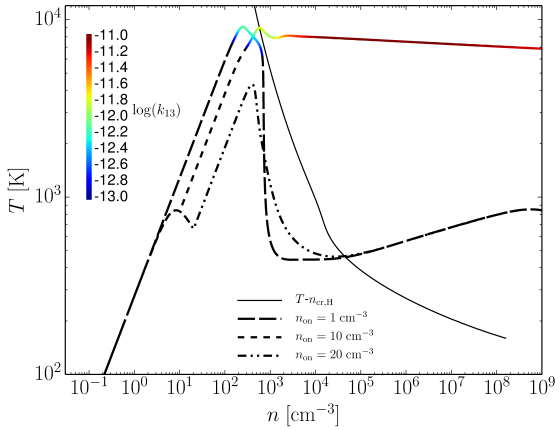

FIG. 13.— The temperature track if the external BH1 radiation field switched on at total number density 1, 10 and 20 cm^{-3} respectively. In the temperature we color the segment where the H_2 collisional dissociation rate $k_{13} > 10^{-13}$ cm^3 s^{-1}. In the same panel we also plot the T-$n_{\rm cr,H}$ curve.

TABLE 3
RATES OF REACTIONS ADOPTED IN THIS WORK.

Ordinal	Reaction	Rate[a,b]		units
(1)	$H + e^- \rightarrow H^+ + 2e^-$	$k_1 = \exp[-32.71396786375$ $+13.53655609057(\ln T_{\rm eV})$ $-5.739328757388(\ln T_{\rm eV})^2$ $+1.563154982022(\ln T_{\rm eV})^3$ $-0.2877056004391(\ln T_{\rm eV})^4$ $+0.03482559773736999(\ln T_{\rm eV})^5$ $-0.00263197617559(\ln T_{\rm eV})^6$ $+0.0001119543953861(\ln T_{\rm eV})^7$ $-2.039149852002 \times 10^{-6}(\ln T_{\rm eV})^8]$		cm^3 s^{-1}
(2)	$He + e^- \rightarrow He^+ + 2e^-$	$k_2 = \exp[-44.09864886561001$ $+23.91596563469(\ln T_{\rm eV})$ $-10.75323019821(\ln T_{\rm eV})^2$ $+3.058038757198(\ln T_{\rm eV})^3$ $-0.5685118909884001(\ln T_{\rm eV})^4$ $+0.06795391233790001(\ln T_{\rm eV})^5$ $-0.005090561018570001(\ln T_{\rm eV})^6$ $+0.0002067236157507(\ln T_{\rm eV})^7$ $-3.649161410833 \times 10^{-6}(\ln T_{\rm eV})^8]$		cm^3 s^{-1}
(3)	$H^+ + e^- \rightarrow H + \gamma$	$k_3 = \exp[-28.61303380689232$ $-0.7241125657826851(\ln T_{\rm eV})$ $-0.02026044731984691(\ln T_{\rm eV})^2$ $-0.002380861877349834(\ln T_{\rm eV})^3$ $-0.0003212605213188796(\ln T_{\rm eV})^4$ $-0.00001421502914054107(\ln T_{\rm eV})^5$ $+4.989108920299513 \times 10^{-6}(\ln T_{\rm eV})^6$ $+5.755614137575758 \times 10^{-7}(\ln T_{\rm eV})^7$ $-1.856767039775261 \times 10^{-8}(\ln T_{\rm eV})^8$ $-3.071135243196595 \times 10^{-9}(\ln T_{\rm eV})^9]$		cm^3 s^{-1}
(4)	$He^+ + e^- \rightarrow He + \gamma$	$k_4 = 1.54 \times 10^{-9}[1 + 0.3/\exp(8.099328789667/T_{\rm eV})]/$ $[\exp(40.49664394833662/T_{\rm eV}) \times T_{\rm eV}^{1.5}]$ $+3.92 \times 10^{-13}/T_{\rm eV}^{0.6353}$		cm^3 s^{-1}
(5)	$H + H^+ \rightarrow {H_2}^+ + \gamma$	$k_5 = 1.85 \times 10^{-23} T^{1.8}$ $k_5 = 5.81 \times 10^{-16}(T/56200)^{[-0.6657\log(T/56200)]}$	$T \leq 6.7 \times 10^3$K $T > 6.7 \times 10^3$K	cm^3 s^{-1}
(6)	$H_2^+ + H \rightarrow H_2 + H^+$	$k_6 = 6.0 \times 10^{-10}$		cm^3 s^{-1}
(7)	$H + e^- \rightarrow H^- + \gamma$	$k_7 = 6.775 \times 10^{-15}(T_{\rm eV})^{0.8779}$		cm^3 s^{-1}
(8)	$H + H^- \rightarrow H_2 + e^-$	$k_8 = 1.43 \times 10^{-9}$ $k_8 = \exp[-20.06913897587003$ $+0.2289800603272916(\ln T_{\rm eV})$ $+0.03599837721023835(\ln T_{\rm eV})^2$ $-0.004555120027032095(\ln T_{\rm eV})^3$	$T_{\rm eV} \leq 0.1$ $T_{\rm eV} > 0.1$	cm^3 s^{-1}

TABLE 3 — Continued

Ordinal	Reaction	Rate[a,b]		units
		$-0.00031051154471240 16(\ln(T_{\rm eV})^4$ $+0.00010732940103672 47(\ln(T_{\rm eV})^5$ $-8.36671960467864\times10^{-6}(\ln T_{\rm eV})^6$ $+2.238306228891639\times10^{-7}(\ln(T_{\rm eV})^7]$		
(9)	$H_2^+ + e^- \rightarrow 2H$	$k_9 = 1\times10^{-8}$ $k_9 = 1.32\times10^{-6}T^{-0.76}$	$T\leq 617$K $T>617$K	cm^3 s^{-1}
(10)	$H_2^+ + H^- \rightarrow H_2 + H$	$k_{10} = 5\times10^{-6}T^{-0.5}$		cm^3 s^{-1}
(11)	$H^- + H^+ \rightarrow 2H$	$k_{11} = 6.5\times10^{-9}T_{\rm eV}^{-0.5}$		cm^3 s^{-1}
(12)	$H_2 + e^- \rightarrow H + H^-$	$k_{12} = 2.7\times10^{-8}T^{-1.27}\exp(-43000/T)$		cm^3 s^{-1}
(13)	$H_2 + H \rightarrow 3H$	see Martin et al. (1996)		cm^3 s^{-1}
(14)	$H_2 + H_2 \rightarrow H_2 + 2H$	$k_{14,\rm L} = 1.18\times10^{-10}\exp(-6.95\times10^4/T)$ $k_{14,\rm H} = 8.125\times10^{-8}T^{-1/2}\exp(-5.2\times10^4/T)[1-\exp(-6\times10^3/T)]$ $\log n_{\rm cr,H_2} = 4.845 - 1.3\log(T/10^4) + 1.62[\log(T/10^4)]^2$ $a = (1+n_{\rm H}/n_{\rm cr,H_2})^{-1}$, $k_{14} = k_{14,\rm H}^{1-a}k_{14,\rm L}^{a}$		cm^3 s^{-1}
(15)	$H_2 + H^+ \rightarrow H_2^+ + H$	$k_{15} = \exp[-24.24914687731536$ $+3.400824447095291(\ln T_{\rm eV})$ $-3.898003964650152(\ln T_{\rm eV})^2$ $+2.045587822403071(\ln T_{\rm eV})^3$ $-0.5416182856220388(\ln T_{\rm eV})^4$ $+0.0841077503763412(\ln T_{\rm eV})^5$ $-0.0078790261544834 55(\ln T_{\rm eV})^6$ $+0.0004138398421504563(\ln T_{\rm eV})^7$ $-9.36345888928611\times10^{-6}(\ln T_{\rm eV})^8]$		cm^3 s^{-1}
(16)	$H_2 + e^- \rightarrow 2H + e^-$	$5.6\times10^{-11}\exp(-102124/T)T^{0.5}$		cm^3 s^{-1}
(17)	$H^- + e^- \rightarrow H + 2e^-$	$k_{17} = \exp[-18.01849334273$ $+2.360852208681(\ln T_{\rm eV})$ $-0.2827443061704(\ln T_{\rm eV})^2$ $+0.01623316639567(\ln T_{\rm eV})^3$ $-0.03365012031362999(\ln T_{\rm eV})^4$ $+0.01178329782711(\ln T_{\rm eV})^5$ $-0.001656194699504(\ln T_{\rm eV})^6$ $+0.0001068275202678(\ln T_{\rm eV})^7$ $-2.631285809207\times10^{-6}(\ln T_{\rm eV})^8]$		cm^3 s^{-1}
(18)	$H^- + H \rightarrow 2H + e^-$	$k_{18} = 2.56\times10^{-9}T_{\rm eV}^{1.78186}$ $k_{18} = \exp[-20.37260896533324$ $+1.139449335841631(\ln T_{\rm eV})$ $-0.1421013521554148(\ln T_{\rm eV})^2$ $+0.00846445538663(\ln T_{\rm eV})^3$ $-0.0014327641212992(\ln T_{\rm eV})^4$ $+0.0002012250284791(\ln T_{\rm eV})^5$ $+0.0000866396324309(\ln T_{\rm eV})^6$ $-0.00002585009680264(\ln T_{\rm eV})^7$ $+2.4555011970392\times10^{-6}(\ln T_{\rm eV})^8$ $-8.06838246118\times10^{-8}(\ln T_{\rm eV})^9]$	$T_{\rm eV}\leq 0.1$ $T_{\rm eV}>0.1$	cm^3 s^{-1}
(19)	$H^- + H^+ \rightarrow H_2^+ + e^-$	$k_{19} = 4\times10^{-4}T^{-1.4}\exp(-15100/T)$ $k_{19} = 1\times10^{-8}T^{-0.4}$	$T\leq10^4$K $T>10^4$K	cm^3 s^{-1}
(20)	$H + H + H \rightarrow H_2 + H$	$k_{20} = 5.5\times10^{-29}T^{-1}$		cm^6 s^{-1}
(21)	$H + H + H_2 \rightarrow H_2 + H_2$	$k_{21} = k_{20}/8$		cm^6 s^{-1}
(22)	$H_2 + \gamma \rightarrow 2H$	see Eq. (14, 17 & 18)		s^{-1}
(23)	$H^- + \gamma \rightarrow H + e^-$	see Eq. (21, 22 & 23)		s^{-1}
(24)	$H_2^+ + \gamma \rightarrow H + H^+$	see Eq. (24, 25 & 26)		s^{-1}

[a] $T_{\rm eV}$ and T are temperature in units eV and K respectively.

[b] Reaction (12) is from Glover & Abel (2008); reaction (14) is from Omukai (2000); reactions (20) and (21) are from Palla et al. (1983); others are from Shang et al. (2010); original references are found in these cited papers.

TABLE 4
HEATING FUNCTIONS USED IN THIS WORK.

Oridinal	Processes	Heating functions[d] [erg cm^{-3} s^{-1}]
(1)[e]	2 body H_2 formation	$\mathcal{H}_{2b} = 1.6\times10^{-12}\{k_8 n_{H^-} n_H[3.53(1+n_{cr}/n_H)^{-1}] + k_6 n_{H_2^+} n_H[1.83(1+n_{cr}/n_H)^{-1}]\}$
(2)	3 body H_2 formation	$\mathcal{H}_{3b} = 1.6\times10^{-12}\times4.48(k_{20} n_H n_H n_H + k_{21} n_H n_H n_{H_2})$

[d] All from Yoshida et al. (2006), original references are found therein.
[e] $n_{cr} = 10^6 T^{-1/2}\left\{1.6 y_H \exp\left[-\left(\frac{400}{T}\right)^2\right] + 1.4 y_{H_2}\exp\left[-\left(\frac{12000}{T+1200}\right)\right]\right\}^{-1}$, y_H and y_{H_2} are H and H_2 number fractions respectively.

TABLE 5
COOLING FUNCTIONS USED IN THIS WORK.

Oridinal	Processes	Cooling functions[f,g] [erg cm^{-3} s^{-1}]
(1)	collisional excitation	$\Lambda_{H_2,n_H\to0} = \mathrm{dex}[-103.0 + 97.59\log T - 48.05(\log T)^2 + 10.80(\log T)^3 - 0.9032(\log T)^4] n_H n_{H_2}$
		$\Lambda_{H_2,LTE} = \left\{6.7\times10^{-19}\exp\left(-\frac{5.86}{T_3}\right) + 1.6\times10^{-18}\exp\left(-\frac{11.7}{T_3}\right) + \frac{9.5\times10^{-22}T_3^{3.76}}{1+0.12T_3^{2.1}}\exp\left[-\left(\frac{0.13}{T_3}\right)^3\right] + 3\times10^{-24}\exp\left(-\frac{0.51}{T_3}\right)\right\} n_{H_2}$
		$\Lambda_{H_2}^{col\text{-}exc} = \frac{\Lambda_{H_2,LTE}}{(1+\Lambda_{H_2,LTE}/\Lambda_{H_2,n_H\to0})}$
(2)	collisional dissociation	$\Lambda_{H_2}^{col\text{-}dis} = 7.2\times10^{-12}(k_{13} n_H + k_{14} n_{H_2}) n_{H_2}$
(3)	recombination	$\Lambda_H^{rec} = 8.7\times10^{-27} T^{0.5} T_3^{-0.2}(1+T_6^{0.7})^{-1} n_e n_{H^+}$
		$\Lambda_{He}^{rec} = 1.55\times10^{-26} T^{0.3647} n_e n_{He^+}$
(4)	collisional ionization	$\Lambda_H^{col\text{-}ion} = 1.27\times10^{-21} T^{1/2}(1+T_5^{0.5})^{-1}\exp\left(-\frac{157809.1}{T}\right) n_e n_H$
		$\Lambda_{He}^{col\text{-}ion} = 9.38\times10^{-22} T^{0.5}(1+T_5^{0.5})^{-1}\exp\left(-\frac{285335.4}{T}\right) n_e n_{He}$
(5)	collisional excitation	$\Lambda_H^{col\text{-}exc} = 7.5\times10^{-19}(1+T_5^{0.5})^{-1}\exp\left(-\frac{118348}{T}\right) n_e n_H$
		$\Lambda_{He}^{col\text{-}exc} = 9.1\times10^{-27} T^{-0.1687}(1+T_5^{0.5})^{-1}\exp\left(-\frac{13179}{T}\right) n_e^2 n_{He^+}$
		$\Lambda_{He^+}^{col\text{-}exc} = 5.54\times10^{-17} T^{-0.397}(1+T_5^{0.5})^{-1}\exp\left(-\frac{473638}{T}\right) n_e n_{He^+}$
(6)	Bremsstrahlung	$\Lambda^{Bre} = 1.42\times10^{-27} T^{0.5}(n_{H^+} + n_{He^+}) n_e$
(7)	Compton	$\Lambda^{com} = 1.017\times10^{-37} T_{CMB}^4 (T - T_{CMB}) n_e$

[f] $T_3 = T/10^3$ K, $T_5 = T/10^5$ K, $T_6 = T/10^6$ K
[g] Function (1) is from Galli & Palla (1998) & Hollenbach & McKee (1979); function (2) from Glover & Jappsen (2007); functions (3) - (5) are from Maselli et al. (2003); functions (6) - (7) are from Maselli et al. (2003); original references are found in these cited papers.